POLITECNICO DI TORINO
Repository ISTITUZIONALE

Dynamics and Control of Helical Arrays in Low Earth Orbit

Original
Dynamics and Control of Helical Arrays in Low Earth Orbit / Apa, R., Quadrelli, M.B., Beauchamp, R.M.. - ELETTRONICO. - (2022), pp. 1-20. (2022 IEEE Aerospace Conference, AERO 2022 Big Sky, MT (USA) 05-12 March 2022) [10.1109/AERO53065.2022.9843283].

Availability:
This version is available at: 11583/2995956 since: 2024-12-27T12:46:34Z

Publisher:
IEEE Computer Society

Published
DOI:10.1109/AERO53065.2022.9843283

Terms of use:

This article is made available under terms and conditions as specified in the corresponding bibliographic description in the repository

Publisher copyright
IEEE postprint/Author's Accepted Manuscript

©2022 IEEE. Personal use of this material is permitted. Permission from IEEE must be obtained for all other uses, in any current or future media, including reprinting/republishing this material for advertising or promotional purposes, creating new collecting works, for resale or lists, or reuse of any copyrighted component of this work in other works.

(Article begins on next page)

08 October 2026

Dynamics and Control of Helical Arrays in Low Earth Orbit

Riccardo Apa
Jet Propulsion Laboratory
California Institute of Technology
4800 Oak Grove Dr., Pasadena, CA 91109
riccardo.apa@jpl.nasa.gov

Marco B. Quadrelli
Jet Propulsion Laboratory
California Institute of Technology
4800 Oak Grove Dr., Pasadena, CA 91109
marco.b.quadrelli@jpl.nasa.gov

Robert M. Beauchamp
Jet Propulsion Laboratory
California Institute of Technology
4800 Oak Grove Dr., Pasadena, CA 91109
robert.m.beauchampb@jpl.nasa.gov

***Abstract*—Spacecraft formation flying is an anticipated critical technology, needed to enhance astrophysical and science missions in near-Earth and interplanetary environments. Enabling a set of distributed spacecraft to corporate together, collectively fulfilling a mission objective, has proven to have several benefits over the conventional large single entity spacecraft. Mission cost and risk are reduced, while the retrieval of scientific data is significantly increased. Augmented adaptability and flexibility will play a crucial role in future space missions which require radar apertures that are excessively large and not practical to built. The key strategic goal of our work is to develop active and passive radar remote sensing applications based on distributed array architectures. Distributed formations of low-cost SmallSats, either deployable or free-flying, can deliver a comparable or greater mission capability than large monolithic spacecraft, but with significantly enhanced flexibility (adaptability, scalability, evolvability, and maintainability) and robustness (reliability, survivability, and fault-tolerance). This research is aligned with the NASA Technology Roadmap for Robotics and Autonomous Systems (TA4), in particular TA4.5 System-Level Autonomy (Activity Planning; Autonomous Guidance and Control; and Multi-Agent Coordination) and TA4.6 Autonomous Rendezvous and Docking.**

This paper outlines the design of a small-satellite helical formation, serving as a Synthetic Aperture Radar (SAR) in low Earth orbit. The macro topic treated in this paper is the analysis of the feasibility and problems related to the operation of autonomous satellite formations serving as a Synthetic Aperture Radar (SAR) in low Earth orbit. An earlier preliminary version of this work was presented recently [1]. The main objective is to control with great precision the relative 6DoF dynamics of the followers with respect to a leader satellite in order to allow a correct taking of the data required by the mission. The differential accelerations to which the formation satellites are subjected make it necessary to implement control techniques for their re-positioning. To ensure a long mission duration, the number of such correction maneuvers should be minimized. In an autonomous formation perspective, such corrections are computed by the spacecrafts themselves, which therefore need to be equipped with sufficient computational resources. In this paper the problems just presented are described in detail and some techniques to mitigate their effects are reported. In order to have results more similar to reality, a high precision dynamic propagation model has been created and validated with the NASA General Mission Analysis Tool (GMAT). This model includes harmonics of the gravitational potential up to order 21, drag, solar pressure and third-body perturbation (Moon and Sun) [2]. After defining the external environment in which the satellites operate, the problem of maintaining the desired configuration of the system is addressed through two different analyzes: uncontrolled dynamics stability analysis and active formation control. The study of uncontrolled formation stability aims to derive the initial conditions of the formation satellites that most closely minimize the relative drift between followers and leader. This allows to reduce the number of maneuvers required to maintain the formation given a fixed interval of time. Despite the careful choice of initial conditions, this drift, although minimal, will tend to alter the initial configuration until the formation is no longer operational. For these reasons, an active control solution, aiming to minimize the amount of fuel used to perform the correction maneuver, has been implemented. The optimal controller is presented in different variants, in particular two strategies, centralized and decentralized, have been implemented in the context of Sequential Convex Programming (SCP). Both types of control were analyzed considering possible un-modeled external factors. Some test cases are reported so that discussion and conclusions can be made regarding the limitations and issues associated with the methodologies implemented.

©2021 California Institute of Technology. Government sponsorship acknowledged. This research was carried out at the Jet Propulsion Laboratory, California Institute of Technology, under a contract with the National Aeronautics and Space Administration
978-1-6654-3760-8/22/$31.00 ©2022 IEEE

TABLE OF CONTENTS

1. INTRODUCTION 1
2. RELATIVE MOTIONS EQUATIONS 2
3. FORMATION STABILITY 4
4. FORMATION CONTROL 13
5. NUMERICAL RESULTS 15
6. CONCLUSIONS 19
ACKNOWLEDGMENTS 19
REFERENCES 19
BIOGRAPHY 20

1. INTRODUCTION

Spacecraft Formation Flying is a technology that has recently undergone a strong development and interest. There are many potentialities of this system, the main ones include an extreme enhanced flexibility (adaptability, scalability, evolvability, and maintainability) and robustness (reliability, survivability, and fault-tolerance). Several missions involving the use of satellites in formation have been performed and many more are expected for future years. A particular application of Formation Flying in remote sensing is Synthetic Aperture Radar (SAR), where high resolution images of the target are reconstructed using satellite motion and signal processing. This concept can be extended in the case of a group of satellites in which there may be separate receiving and

transmitting satellites, or satellites in which receiver and transmitter are mounted on the same platform. The quality of the data, the resolution of the images and the interferometric pattern that is created on the ground depend on multiple factors. Among the most important, the relative geometry between the satellites of the system plays a crucial role. The concept of the *baseline* is of substantial importance and is used as a parameter to define the performance of the system. The accurate maintenance of relative distances and velocities is therefore essential for obtaining high quality data. This work aims to perform a feasibility analysis of the system, presenting the main problems related to Formation Flying for Remote sensing applications. In order to do so, the problem is treated from the deployment, defining the initial conditions of each satellite until the active control of the formation. The satellites that are part of a distributed orbiting system are continuously subject to differential accelerations that tend to "break" the initial configuration of the system (drift) thus decreasing the quality of the data taken. The modeling of these perturbations can be more or less accurate depending on the accuracy requirements of the system and the relevance of this perturbation compared between them. In the case of low orbit (LEO), the main perturbations are Earth's oblateness (J2-effect), atmospheric drag, and solar radiation pressure. In the present work, an orbital propagation model that takes into account the gravity potential up to order 21, atmospheric drag with Harris-Priester density model, solar pressure with conical shadow model and third-body perturbation (Sun and Moon) has been developed and validated with NASA General Mission Analysis Tool (GMAT) in order to have high precision simulations. This type of system obtains particular advantages when the formation is constituted by small-satellites that represent an economic solution and at the same time fault-tolerant that increase the capacity of the system. In this case, however, two main problems arise: the possibility of embarking little propellant to perform the maneuvers and less computational resources. The first problem can be treated in two ways. The first considers the stability of the formation during a propagation of uncontrolled dynamics. This analysis aims to find initial conditions in terms of initial relative positions and velocities such that the formation undergoes minimal drift when no control action is acting. This methodology is based on the equivalence of the energies of the orbits of the different satellites in the formation and goes by the name of Energy Matching [16]. The second way involves an active control of the formation. In this situation, the synthesis of the control laws should be able to take into account the fuel utilization, trying to minimize an objective function by exploiting the dynamics of the system. The second problem can be addressed through the use of algorithms that are computationally eco-friendly. Moreover, in addition to the intrinsic characteristics of the algorithm, the choice of the computational strategy, centralized or de-centralized, turns out to be of fundamental importance for the feasibility of the mission. Despite the precautions taken in the choice of initial conditions, formation control algorithms will be necessary for the correct maintenance of the formation configuration. In this work optimal controller has been analyzed in view of Sequential Convex Programming (SCP) in a centralized and de-centralized strategy [8]. A 6DoF dynamics control will be performed in order to take into account the system performance when specific pointing is required. Regarding the organization of this work, Section 2 reports the main characteristics of relative dynamics, both for translational and rotational dynamics, by presenting the equations governing the relative motion description of a 6-DoF satellite with respect to a chief spacecraft. Section 3 presents one of the main issue related to Formation Flying, i.e. the stability of the formation. The topic is widely discusses by introducing principal configurations used for remote sensing purposes. These configurations will prove as practical test cases which will help showing the behaviors of free-flying formations subject to different relative initial conditions. Section 4 presents the optimal controller mentioned above. Section 5 presents test cases through which it is possible to analyze the performances of the different methodologies presented. Finally, Section 6 reports a brief discussion on the results achieved and outlines possible future research which could represent an appropriate continuation of this work.

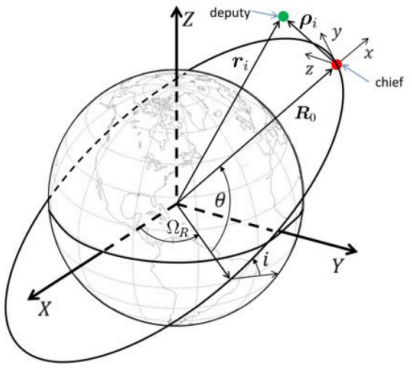

Figure 1. Chief and deputy LVLH frame description, [26]

2. RELATIVE MOTIONS EQUATIONS

Relative motion is usually described in LVLH frame. Many works in literature focused on deriving the equation of motion of the LVLH frame. In particular, since LVLH frame is a non-inertial frame, the efforts have been focused on deriving its angular velocity $\boldsymbol{\Omega}$ and acceleration $\dot{\boldsymbol{\Omega}}$ vectors which are essential for the description of the relative motion. Analytical solutions to this problem has been found by [15] considering a LVLH affected only by J_2 perturbation and by [18] for a LVLH affected by J_2 and Drag perturbations. In this work the solution considering only J_2 perturbation has been used and it proved sufficiently accurate for the reasons this frame is usually implied for.

Figure 1 shows the main elements involved in the description of the relative motion involving two satellites, a chief and a deputy. The chief is the satellite the dynamics is described with respect to. Its center of mass is the origin of LVLH frame and it can be a real satellite or a virtual one, in the latter case it is not forced to undergo all the perturbations the deputy is subjected to. In fact, it is used as a local observer whose main purpose is to be able to describe the motion considering relative distances and velocities, which are the controlled quantities in formation flying. The deputy is a real satellite whose motion has to be described relatively to the chief. Using the notation present in Figure 1, the following equation can be easily derived

$$\boldsymbol{\rho}_i = \boldsymbol{r}_i - \boldsymbol{R}_0 \tag{1}$$

where $\boldsymbol{R}_0$ is the ECI position vector of the chief spacecraft, $\boldsymbol{\rho}_i$ is the relative position vector of the deputy spacecraft with respect to the chief and $\boldsymbol{r}_i$ is the ECI position vector of the deputy.

Relative Translational Dynamics Modeling

There are two possible ways to obtain the relative quantities of a spacecraft relative to another. In fact, it is always possible to integrate dynamic equations separately for each spacecraft and then use the description of the motion with respect to a non-inertial frame in order to find relative position, velocity and acceleration seen by LVLH frame in LVLH components [4]. The second methodology, which has been used in this paper, is to integrate directly the relative dynamics equations in LVLH frame. Deriving two times the left side of Equation 1 in LVLH frame, it is possible to obtain

$$\begin{aligned}\ddot{\boldsymbol{\rho}}_{i,L} =&\boldsymbol{R}_{LI}(\ddot{\boldsymbol{r}}_{i,I} - \ddot{\boldsymbol{R}}_{0,I}) - \boldsymbol{\Omega}_L \times \boldsymbol{\Omega}_L \times \boldsymbol{\rho}_{i,L} \\ &- \dot{\boldsymbol{\Omega}}_L \times \boldsymbol{\rho}_{i,L} - 2\boldsymbol{\Omega}_L \times \dot{\boldsymbol{\rho}}_{i,L}\end{aligned} \tag{2}$$

Where in particular $\boldsymbol{\Omega}_L$ and $\dot{\boldsymbol{\Omega}}_L$ are the angular velocity and acceleration of LVLH frame with respect to ECI written in LVLH components, $\boldsymbol{R}_{LI}$ is the transformation matrix from ECI to LVLH frame, $(\ddot{\boldsymbol{r}}_{i,I} - \ddot{\boldsymbol{R}}_{0,I})$ represents the difference between inertial accelerations of the deputy and the chief expressed with components in inertial frame and $\boldsymbol{\rho}_{i,L}$ is the relative position vector of the deputy spacecraft with respect to the chief described in LVLH frame. This second approach results in a more practical way of describing the relative motion, in fact, it is possible to impose relative initial and final condition in a simpler way, this makes the control algorithm simpler and more evident having in mind that relative position and velocity vectors are the quantities of interest.

Rotational Dynamics Modeling

Concerning rotational motion, it is also possible to describe the relative attitude between the deputy and chief spacecrafts, in particular, in [11], the dynamics equation for the relative angular accelerations between the body-frames of two different spacecrafts is found. This approach can prove very useful in many applications, especially for those which need to know relative position between any two points of two spacecrafts which are not the center of mass. In fact, assuming the approximations of rigid bodies, thanks to relative rotational dynamics it is possible to calculate the velocity and acceleration of any point of the spacecraft by knowing the position vector with respect to the center of mass. Examples of this kind of applications are tethered systems [13] [12] [14], [5], in which the links between tethers do not necessarily pass through the center of mass or systems which present instruments for relative dynamics metrology that have to be positioned in the external surfaces of the spacecraft [19] [20] and whose position has to be known in order to improve the precision of the calculations they perform. In other kind of application, like in case of Earth system monitoring [6] or Interferometry [17], it can be useful to derive the equations of absolute rotational dynamics, i.e. it is convenient to have the relative attitude between the body-frame and the inertial frame. In this work, this second way of describing rotational dynamics has been pursued, it is possible to write for each spacecraft the following equation assuming that the body is not flexible ($\frac{d}{dt}\boldsymbol{J}_G = 0$), referring the equation to a moving frame (the body frame) and solving for the angular velocity

$$\begin{aligned}\dot{\boldsymbol{\omega}}_{BF} =&\boldsymbol{J}_{G,BF}^{-1}(\sum_j \boldsymbol{\tau}_{j,BF}^{pert} + \sum_k \boldsymbol{\tau}_{k,BF}^{int} - \sum_i \dot{\boldsymbol{h}}_{i,BF} \\ &- \boldsymbol{\omega}_{BF} \times (\boldsymbol{J}_{G,BF}\boldsymbol{\omega}_{BF} + \sum_i \boldsymbol{h}_{i,BF}))\end{aligned} \tag{3}$$

where $\boldsymbol{J}_{G,BF}$ is the moment of inertia matrix with respect to the considered frame whose origin coincides with the center of mass of the body and $\boldsymbol{\omega}_{BF}$ is the angular velocity of the body-frame with respect to inertial frame, $\boldsymbol{h}_{i,BF}$ denotes the i-th internal angular momentum (reaction wheels etc..), $\boldsymbol{\tau}_{j,BF}^{pert}$ denotes the j-th perturbation torque, $\boldsymbol{\tau}_{k,BF}^{int}$ denotes the k-th unwanted internal torque and pedex BF underines that the components in the body-frame are considered.

In this work, the attitude has been represented by unitary quaternion $\boldsymbol{q} = q_1\hat{\boldsymbol{i}}+q_2\hat{\boldsymbol{j}}+q_3\hat{\boldsymbol{k}}+q_4$. The kinematics equation holds

$$\dot{\boldsymbol{q}}_{BF} = \frac{1}{2}W(\boldsymbol{\omega}_{BF})\boldsymbol{q}_{BF} \tag{4}$$

where the notation $\boldsymbol{q}_{BF}$ underlines that the quaternion components are expressed in body-frame and

$$W(\boldsymbol{\omega}) = \begin{bmatrix} 0 & \omega_z & -\omega_y & \omega_x \\ -\omega_z & 0 & \omega_x & \omega_y \\ \omega_y & -\omega_x & 0 & \omega_z \\ -\omega_x & -\omega_y & -\omega_z & 0 \end{bmatrix} \tag{5}$$

Equations 4 and 3 will be used in the next section for deriving the general non-linear dynamics system describing the relative motion of all the formation.

Non-Linear Complete State Space Representation

Now that both the translational motion equations and rotational ones have been reported, it is possible to write the non-linear system whose integration returns relative position and velocities with respect to the LVLH frame and attitude and angular velocities of the body-frame with respect to a Inertial frame for each spacecraft of the formation.
In a free-flying configuration, each spacecraft is dynamically independent from the others, so applying Equations 2 and 3 to the single spacecraft and defining the state vector in the following way

$$\boldsymbol{X}_i = \begin{pmatrix} \boldsymbol{\rho}_i \\ \dot{\boldsymbol{\rho}}_i \\ \boldsymbol{q}_{BF} \\ \boldsymbol{\omega}_{BF} \end{pmatrix} \tag{6}$$

it is possible to obtain non-linear dynamical system for each spacecraft

$$\dot{\boldsymbol{X}}_i = f_i(\ddot{\boldsymbol{r}}_i, \ddot{\boldsymbol{R}}_0, \boldsymbol{\Omega}, \dot{\boldsymbol{\Omega}}, \boldsymbol{X}_i) \tag{7}$$

where the dependence on the inertial accelerations of the spacecraft and LVLH frame, and its angular velocity and acceleration has been highlighted. The suffix i indicates that all quantities in f are referred to the i-th spacecraft. It is possible to expand 7 as

$$f_i = \begin{pmatrix} \frac{d}{dt}\boldsymbol{\rho}_{i,L} \\ \\ \boldsymbol{R}_{LI}(\ddot{\boldsymbol{r}}_{i,I} - \ddot{\boldsymbol{R}}_{0,I}) - \boldsymbol{\Omega}_L \times \boldsymbol{\Omega}_L \times \boldsymbol{\rho}_{i,L} \\ -\dot{\boldsymbol{\Omega}}_L \times \boldsymbol{\rho}_{i,L} - 2\boldsymbol{\Omega}_L \times \dot{\boldsymbol{\rho}}_{i,L} \\ \\ \frac{1}{2}W(\boldsymbol{\omega}_{BF})\boldsymbol{q}_{BF} \\ \\ \boldsymbol{J}_{G,BF}^{-1}(\sum_j \boldsymbol{\tau}_{j,BF}^{pert} + \sum_k \boldsymbol{\tau}_{k,BF}^{int} - \sum_i \dot{\boldsymbol{h}}_{i,BF} \\ -\boldsymbol{\omega}_{BF} \times (\boldsymbol{J}_{G,BF}\boldsymbol{\omega}_{BF} + \sum_i \boldsymbol{h}_{i,BF})) \end{pmatrix}$$

In order to be able to integrate Equation 7, the quantities $\ddot{\boldsymbol{r}}_{i,I}$ and $\ddot{\boldsymbol{R}}_{0,I}$ are needed. Concerning $\ddot{\boldsymbol{R}}_{0,I}$ a brief discussion has

been done at the beginning of the section, while concerning $\ddot{\boldsymbol{r}}_{i,I}$ the following holds

$$\ddot{\boldsymbol{r}}_{i,I} = \ddot{\boldsymbol{r}}_{GP,i} + \ddot{\boldsymbol{r}}_{D,i} + \ddot{\boldsymbol{r}}_{SP,i} + \ddot{\boldsymbol{r}}_{TB,Moon,i} + \ddot{\boldsymbol{r}}_{TB,Sun,i}$$

The absolute acceleration of the single satellite is mainly due to the gravity potential (GP), the atmospheric resistance (D), the solar pressure (SP) and the third-body perturbation (TB) (Moon and Sun). The more accurate are the models of each of the individual accelerations the more accurate will be the simulations. The perturbations are function of the absolute inertial position $\boldsymbol{r}_{i,I}$ and velocity $\dot{\boldsymbol{r}}_{i,I}$ that are not available a priori from the state vector $\boldsymbol{X}_i$, but they can easily be computed as follows

$$\boldsymbol{r}_{i,I} = \boldsymbol{R}_{IL}\boldsymbol{\rho}_{i,L} + \boldsymbol{R}_{0,I} \tag{8}$$

$$\dot{\boldsymbol{r}}_{i,I} = \boldsymbol{R}_{IL}\dot{\boldsymbol{\rho}}_{i,L} + \boldsymbol{\Omega}_I \times (\boldsymbol{R}_{IL}\boldsymbol{\rho}_{i,L}) + \dot{\boldsymbol{R}}_{0,I} \tag{9}$$

where $\boldsymbol{R}_{IL}$ is the transformation matrix from LVLH to inertial frame, and $\boldsymbol{\Omega}_I$ is the angular velocity of the LVLH with respect to Inertial frame in inertial components (i.e. $\boldsymbol{\Omega}_I = \boldsymbol{R}_{IL}\boldsymbol{\Omega}_L$). Now it is possible to write the complete system which considers the entire formation dynamics with respect to LVLH frame. If N denotes the number of satellites composing the formation, the system can be written as

$$\begin{pmatrix} \dot{\boldsymbol{R}}_0 \\ \ddot{\boldsymbol{R}}_0 \\ \dot{\boldsymbol{X}}_1 \\ \vdots \\ \dot{\boldsymbol{X}}_N \end{pmatrix} = \begin{pmatrix} \frac{d}{dt}\boldsymbol{R}_0 \\ \sum_j \boldsymbol{a}_{j,I} \\ f_1(\ddot{\boldsymbol{r}}_1, \ddot{\boldsymbol{R}}_0, \boldsymbol{\Omega}, \dot{\boldsymbol{\Omega}}, \boldsymbol{X}_1) \\ \vdots \\ f_N(\ddot{\boldsymbol{r}}_N, \ddot{\boldsymbol{R}}_0, \boldsymbol{\Omega}, \dot{\boldsymbol{\Omega}}, \boldsymbol{X}_N) \end{pmatrix} \tag{10}$$

where $\sum_j \boldsymbol{a}_{j,I}$ indicates the sum in inertial frame of the accelerations acting on the chief spacecraft. Given a set of initial conditions, it is possible to integrate Equation 10 to obtain the relative dynamics at each instant of the integration interval. It is good to remark that Equation 10 does not consider the control laws which will be presented in Section 4, so it describes just the free-flying motion.

3. FORMATION STABILITY

Considering that the spacecrafts are subject to the perturbations, they tend to drift apart from their assigned position so decomposing the desired structure of the entire formation. It is possible to correct periodically this drift by using some active control techniques, some of them analyzed in Section 4, but this requires the use of energy coming from stored propellant. As mentioned in the introduction, the satellites are equipped with a limited amount of propellant, which implies a tendency to reduce these corrections to a minimum in order to extend the duration of the mission. The capability of the formation to maintain its initial relative positions without external control actions is called *Stability*. In this section, passive techniques which have the purpose of improving the stability of the formation are analyzed. In particular, the Initial Relative Conditions (IRC) of the followers with respect to the chief represent the most important aspect to consider when designing a long-lasting mission. These conditions can be divided into Initial Relative Positions (IRP) and Initial Relative Velocities (IRV). IRP are usually fixed by external constraints, the main one is the kind of data the mission is designed to take. IRP define the configuration of the formation, and they often represent the principal quantities control algorithms aim at keeping constant. While IRV are usually chosen to improve the stability. The objectives of this section are to present some of the most used configurations for remote sensing and the problems on the stability of the formation related to non-correct initial conditions. Then, the method of the *Energy Matching* which describes how to derive correct IRC is reported. Finally, some results quantifying how this method improved the stability of the presented configurations are showed and discussed.

Clohessy-Wiltshire IRC

The most important relative dynamics equations derivation can be attributed to Clohessy-Wiltshire (CW equations) [23]. They obtained the equations in a simple case, i.e. they derived relative motion equations of a target (a follower in our case) moving in a circular orbit with respect to a chaser (LVLH frame or chief in our case) following an elliptical or circular orbit. The CW equations, usually written for the uncontrolled propagation (appropriate for a stability analysis), have the following analytical solution:

$$\begin{aligned} \boldsymbol{\rho}(t) &= \Phi_{\rho\rho}(t)\,\boldsymbol{\rho}_0 + \Phi_{\rho\dot{\rho}}(t)\,\dot{\boldsymbol{\rho}}_0 \\ \dot{\boldsymbol{\rho}}(t) &= \Phi_{\dot{\rho}\rho}(t)\,\boldsymbol{\rho}_0 + \Phi_{\dot{\rho}\dot{\rho}}(t)\,\dot{\boldsymbol{\rho}}_0 \end{aligned} \tag{11}$$

$$\Phi_{\rho\rho}(t) = \begin{bmatrix} 4 - 3\cos nt & 0 & 0 \\ 6(\sin nt - nt) & 1 & 0 \\ 0 & 0 & \cos nt \end{bmatrix}$$

$$\Phi_{\rho\dot{\rho}}(t) = \begin{bmatrix} \frac{1}{n}\sin nt & \frac{2}{n}(1 - \cos nt) & 0 \\ \frac{2}{n}(\cos nt - 1) & \frac{1}{n}(4\sin nt - 3nt) & 0 \\ 0 & 0 & \frac{1}{n}\sin nt \end{bmatrix}$$

$$\Phi_{\dot{\rho}\rho}(t) = \begin{bmatrix} 3n\sin nt & 0 & 0 \\ 6n(\cos nt - 1) & 0 & 0 \\ 0 & 0 & -n\sin nt \end{bmatrix}$$

$$\Phi_{\dot{\rho}\dot{\rho}}(t) = \begin{bmatrix} \cos nt & 2\sin nt & 0 \\ -2\sin nt & 4\cos nt - 3 & 0 \\ 0 & 0 & \cos nt \end{bmatrix}$$

where n is the orbital rate of the target, $\boldsymbol{\rho}(t) = [x(t), y(t), z(t)]$ is the position vector, $\boldsymbol{\rho}_0$ and $\dot{\boldsymbol{\rho}}_0$ are the initial position and velocity of the target with respect to to the chaser (the pedex L indicating that the vectors are referred to LVLH frame has been omitted to lighten the notation). The approximations used by this derivation become relevant when the distance between target and chaser increases or when the circularity assumption on the target's orbit is not satisfied. The literature is full of works trying to improve Equations 11 deriving the relative dynamics for arbitrary near-circular orbits subject to J_2 perturbing potential [6] or the state transition matrix of relative motion for the perturbed non-circular reference orbit [7]. Further details on the variety of the works accomplished in this domain can be found in [10].

In the context of this work, Equations 11 are not appropriate to describe the evolution of relative positions and velocities but they can prove very useful to find initial relative parameters to give to the followers in order to create a desired configuration.

In fact, it is possible to re-write the components of equations 11 in terms of differential Keplerian elements as follows [22]

$$\begin{aligned} x_i(t) &= -a \cdot \delta e_i \cos(nt - \alpha_i) \\ y_i(t) &= 2a \cdot \delta e_i \sin(nt - \alpha_i) + a \cdot \delta\theta_i \\ z_i(t) &= a \cdot \delta i_i \sin(nt - \beta_i) \end{aligned} \tag{12}$$

in particular, Equations 12 describe respectively the relative radial, relative along-track and relative across-track evolution

of the i-th follower with respect to chief spacecraft (or the LVLH frame) given the differential orbit inclination δi_i, eccentricity δe_i and argument of latitude $\delta\theta_i$. In addition, a is the semi-major axis of the chief and α_i and β_i define respectively the initial phase angles in xy and z planes.
From Equations 12 it is clearer that in the context of CW assumptions the relative radial and along-track motion is decoupled from the across-track motion. A very important remark is that in xy plane the relative motion describe an ellipse centered at $[x_i, y_i] = [0, \delta\theta_i]$ while in the z one the motion in simply harmonic. It is simple to obtain the components of relative velocity vector $\dot{\boldsymbol{\rho}}_i$ by deriving Equations 12

$$\begin{aligned} \dot{x}_i(t) &= a \cdot \delta e_i n \sin(nt - \alpha_i) \\ \dot{y}_i(t) &= 2a \cdot \delta e_i n \cos(nt - \alpha_i) \\ \dot{z}_i(t) &= a \cdot \delta i_i n \cos(nt - \beta_i) \end{aligned} \tag{13}$$

As stated before, Equations 12 and 13 are not accurate to describe relative motions in general case, it will be necessary to integrate the system 10, but it is possible to use them in order to set the parameters δe_i, α_i, $\delta\theta_i$, δi_i and β_i to correctly initialize position and velocities of a formation given a desired configuration. It is sufficient to evaluate the equations at $t = 0$ to obtain the IRC for the i-th spacecraft

$$\begin{aligned} x_i(0) &= -a \cdot \delta e_i \cos(-\alpha_i) \\ y_i(0) &= 2a \cdot \delta e_i \sin(-\alpha_i) + a \cdot \delta\theta_i \\ z_i(0) &= a \cdot \delta i_i \sin(-\beta_i) \\ \dot{x}_i(0) &= a \cdot \delta e_i n \sin(-\alpha_i) \\ \dot{y}_i(0) &= 2a \cdot \delta e_i n \cos(-\alpha_i) \\ \dot{z}_i(0) &= a \cdot \delta i_i n \cos(-\beta_i) \end{aligned} \tag{14}$$

Equations 14 will be used to initialize some configurations which are mostly used for remote sensing, then the stability of these configurations will be tested.

Remote Sensing Configurations

Formation Flying is a particularly interesting system for remote sensing purposes. The literature presents many studies on this subject [22] [9], in particular, applications of the system working as Synthetic Aperture Radar (SAR) have been studied in the last years. Such a system aims at creating a high-resolution image by using the motion of platform on which the equipment is mounted on. The working principle consists in sending multiple radar pulses in the direction of the target from an initial location, and then in recapturing the echo of the pulses at a different locations in space; signal processing is needed to combine recordings from these multiple antenna positions to create the final image. As the name SAR suggests, this process simulates data taking of a large antenna whose aperture is from hundreds or thousands of meters. The system just described can be implemented in monostatic, bistatic or multistatic approaches. Monostatic consists in a single platform which works both as transmitter and receiver, sending and collecting the pulses it has previously generated (as described above). Bistastic and multistatic approaches are those of interest for Formation Flying because more than one platform is involved in the process. In fact, in the first case, the transmitter and receiver antennas are mounted on different platforms, the transmitter has the purpose of illuminating the scene and the receiver collects the echoes in order to create the image (Figure 2). Multistatic radars extend this concept by using multiple receivers and/or transmitters in order to take more captures making more reliable the target characterization. They can be used in several different configurations. Most used are the *Fully-active* configuration, in which all spacecrafts act as a monostatic radar by sending and receiving the pulses

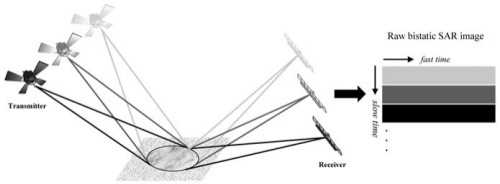

Figure 2. Bistatic radar working principle, [22]

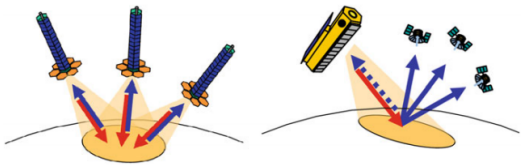

Figure 3. Multistatic radar working principle. *Left:* Fully-active configuration. *Right:* Semi-active configurations, [22]

themselves have generated or the *Semi-active* configuration in which one transmitter illuminates the scene and multiple receivers collect the echoes (Figure 3). From Figures 2 and 3, it is evident that a fine control of relative position between spacecrafts is required to improve data quality. In particular, one of the most important quantity to control in such a system to improve performances is the *Baseline* between the spacecrafts of the formation. Considering two spacecrafts of the formation it is possible to define the baseline as the distance between satellites-target conjunctions. *Baseline* is of relevant importance for the resulting interferometric ground patterns created by the antennas which ultimately imply the type of measurements and the trend of the Signal to Noise Ratio (SNR) as function of the terrain characteristics.
It is now possible to analyze the configurations more used in this domain so that practical examples can help in the understanding of the much more general logical process with which it is wanted to carry out the design of the GN&C system and of the problems associated with it.

Interferometric Cartwheel (IC) Configuration

Interferometric Cartwheel is a well-known configuration in which the satellites of the formation move in the same orbital plane. Considering the parameters introduced in CW initial conditions Equation 14, the last statement implies $\delta i_i = 0$ (so that separation in cross-track plane is equal to 0). In addition, the relative eccentricities of the followers with respect to the chief is equal for all the spacecrafts ($\delta e_i = \delta e$) ensuring the same amplitude of the motion in the xy plane elliptic motion. Finally, in order to have an interferometric baseline it is necessary to decide the initial phasing of each spacecraft (α_i). This can be done according to different criteria but usually an equal spacing between the followers is the one that guarantees a lower risk of collision. In this configuration it is not necessary to give an initial differential argument of latitude $\delta\theta_i$ because the phasing above mentioned guarantees in principle the non-intersection of trajectories. It is then possible to summarize the parameters setting through the following equations:

$$\begin{aligned} \delta i_i &= 0 \\ \delta e_i &= \delta e \qquad\qquad i = 1, 2, ...N \\ \alpha_i &= \alpha_1 + \tfrac{2\pi}{N}(i-1) \\ \delta\theta_i &= 0 \end{aligned} \tag{15}$$

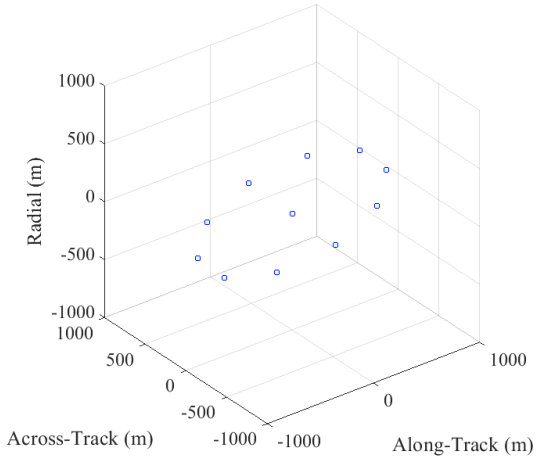

Figure 4. 3D representation of IC configuration

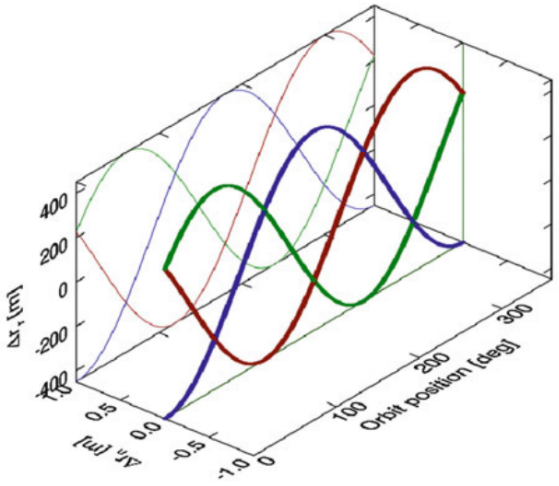

Figure 5. Time-evolution of IC configuration, [22]

where N is the number of the followers spacecrafts (considering that a chief spacecraft could be place at the center of the formation) and α_1 is an arbitrary start phase angle of the first follower. It is possible to visualize a 3D representation of the Interferometric Cartwheel configuration composed by 11 satellites in Figure 4 presenting the leader at the center of the formation. Regarding its time-evolution, in Figure 5 (where Δr_r, Δr_t, Δr_t are the radial, along-track and across-track relative positions) it is visible as the initial conditions give by Equation 15 have the effect of maintaining the motion in xy plane. The advantages of this configuration comprise a good stability of the maximum baseline along the orbit with a small variation and a little across-track drift which usually is the drift which implies a greater amount of fuel consumption to be corrected with respect to along-track and radial drifts.

Cross-Track Pendulum (CTP) Configuration

Cross-Track Pendulum is one of the most used configuration for remote sensing applications. It can be said that it represents the opposite case to the IC configuration. In fact, in this case the satellites present a separation in across-track direction through a differential inclination equal for all the spacecrafts ($\delta i_i = \delta i$) with respect to that of the chief. Regarding instead the eccentricity, this configuration foresees

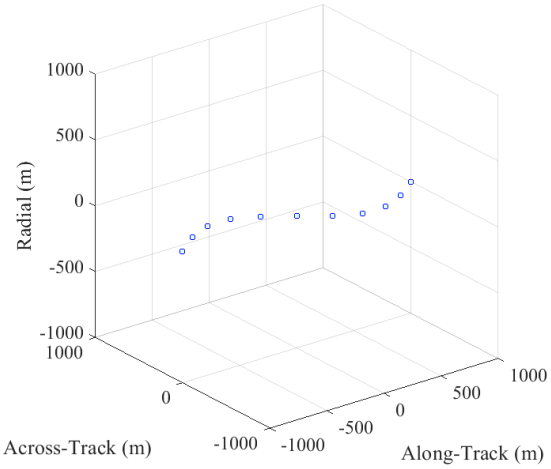

Figure 6. 3D representation of CTP configuration

$\delta e_i = 0$ cancelling in this way a difference in radial direction (the motion results therefore confined to the plane yz). In this case, however, it is necessary to give a separation in along-track directions through a difference in argument of latitude $\delta\theta_i$ in order to avoid collisions. Finally, in order to obtain a baseline in cross-track direction it is necessary to give a difference in β_i. Analogously to the previous case, the choice of equispaced phasing is normally used to minimize the risk of collision. Finally, this configuration is determined by:

$$\begin{array}{c} \delta i_i = \delta i \\ \delta e_i = 0 \\ \beta_i = \beta_1 + \frac{2\pi}{N}(i-1) \\ \delta\theta_i \neq 0 \end{array} \qquad i = 1, 2, ...N \tag{16}$$

Where β_1 is an arbitrary start phase angle and the choice of $\delta\theta_i$ depends on the application. In Figure 6 it is possible to see a 3D visualization of the initial CTP configuration composed by 11 spacecrafts with the leader placed at the center. Instead, the time-evolution for a three satellites case is reported in Figure 7 where it is visible the only yz plane motion and the baselines created in radial direction. The main advantage of CTP is the possibility to have constant along-track baselines, while one of the major disadvantage is that the difference in inclination leads to a differential precession of the RAAN, thus implying a relatively significant drift in across-track direction after a few orbits.

Helix Configuration

In the most general case, Equations 11 create an Helix with respect to the leader. In simple case, the satellite have the same differential eccentricities and inclination which guarantees separation with respect to all planes making this configuration particularly safe with no need for differential argument of latitude, and equispaced phasing in xy plane at z direction. In addition, the cross-track and along-track baselines can be easily changed with a relatively low fuel consumption allowing for a multi-objectives mission. The equations of the parameters for composing the Helix configuration are:

$$\begin{array}{c} \delta i_i = \delta i \\ \delta e_i = \delta e \\ \alpha_i = \alpha_1 + \frac{2\pi}{N}(i-1) \\ \alpha_i = \beta_i \\ \delta\theta_i = 0 \end{array} \qquad i = 1, 2, ...N \tag{17}$$

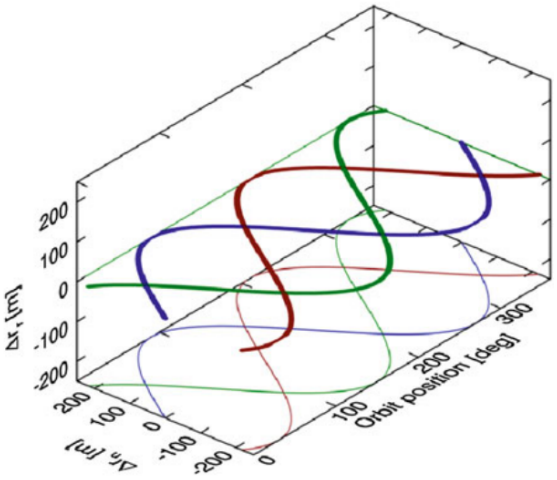

Figure 7. Time-evolution of CTP configuration, [22]

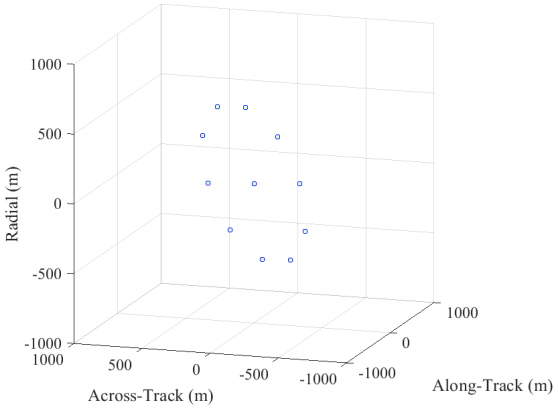

Figure 8. 3D representation of Helix configuration

Where α_1 is the arbitrary start phase angle. In Figure 8 is possible to visualize a 11 spacecrafts Helix configuration. Concerning the time-evolution of the configuration, Figure 9 presents the most simple Helix case with only two spacecrafts, used in TanDEM-X mission [17]. This configuration allows for a cross-track baseline that never nullifies (except in case of only two spacecrafts where it nullifies in two different instants during the orbit) which is also the cause of unwanted differential RAAN precession.

Stability of the CW Initial Conditions

In this section the stability of the presented configurations initialized with Equations 11 is analyzed. In particular, each configuration is propagated with the accurate propagation model accounting for the perturbations mentioned above in order to monitor the evolution of relative distances in the three directions. In the ideal case, the drift with respect to the leader of each spacecraft should be small over the course of hundreds of orbits so that corrections are kept to a minimum. In the following simulations, the initial leader orbital elements are those presented in Table1.

IC free-flying CW Initial Conditions stability

In Figure 10 it is possible to visualize relative propagation of Interferometric Cartwheel configuration present in Figure 4 initialized with CW initial conditions and parameters as

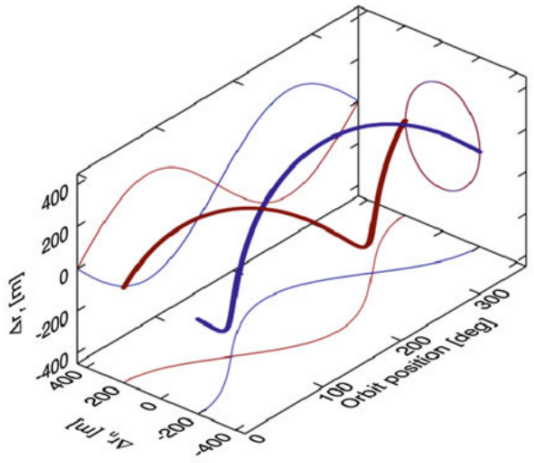

Figure 9. Time-evolution of Helix configuration, [22]

a	$6.94761 \times 10^6 m$
e	0.01
i	97°
Ω	270°
ω	70°
ν	0°

Table 1. Initial Orbital Parameters of the Leader spacecraft

in Table 2. After 80 orbits, relative radial and across-track drift is limited, approximately in the worst case, radial drift is of 2.5 $m/orbit$ while across-track one is only 3.8×10^{-2} $m/orbit$. On the other hand, as far as along-track stability is concerned, the initial conditions used result in an exaggerated drift (about 100 $m/orbit$) that would require frequent corrections in order to restore the initial configuration, greatly decreasing the maximum possible mission duration.

$a \cdot \delta e$	100 m
α_1	9°
N	10

Table 2. IC parameters for simulation.

CTP free-flying CW Initial Conditions stability

Cross-Track Pendulum configuration presented in Figure 6 has a very similar behavior with respect to the IC one. Figure 11 reports the results of relative positions for a 80 orbits simulation using parameters of the configuration as in Table 3. Also in this case, radial and across-track drifts are quite limited, about 0.38 $m/orbit$ for radial drift and 1.25 $m/orbit$ for across-track one. Along-track drift has the opposite direction with respect to IC configuration, in fact, spacecrafts trajectories tend to converge towards the chief spacecraft, this behavior is not acceptable because, if not corrected, could lead the spacecrafts to multiple collisions after only 40 orbits. It is possible to affirm that, in terms of fuel consumption, CTP configuration initialized through Equations 11, is more sustainable than IC one, but not still feasible for long-duration missions.

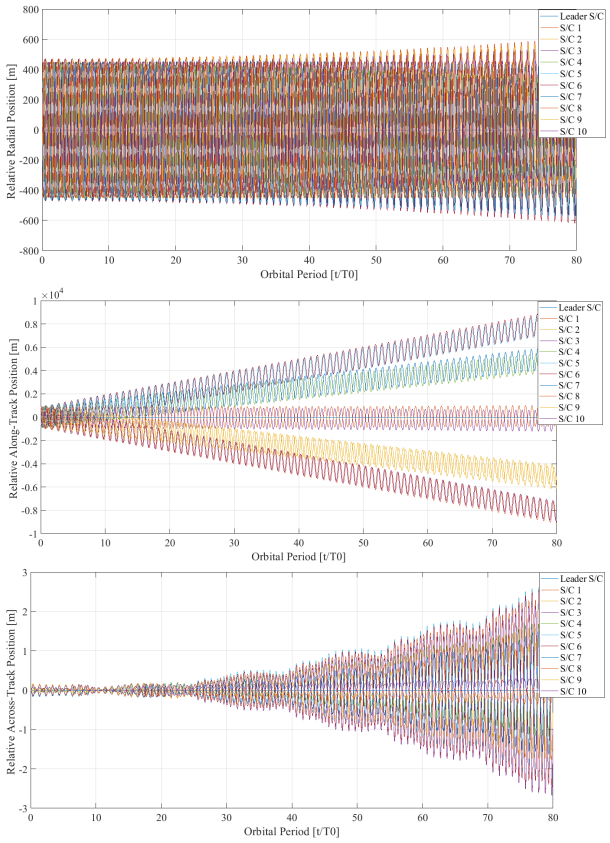

Figure 10. IC relative dynamics propagation, CW Initial Conditions

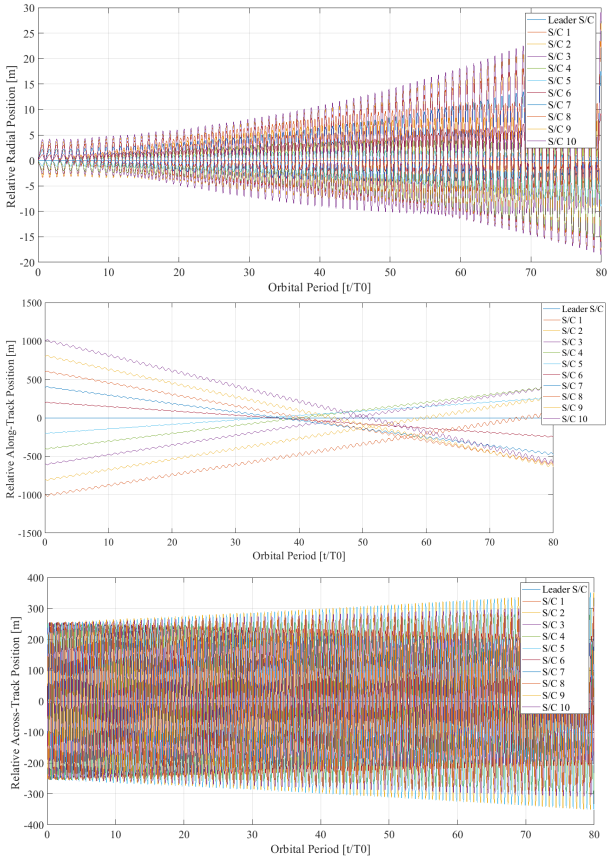

Figure 11. CTP relative dynamics propagation, CW Initial Conditions

$a \cdot \delta i$	$250\ m$
β_1	$9°$
N	10
$a \cdot \delta\theta$	$200\ m$

Table 3. CTP parameters for simulation.

Helix free-flying CW Initial Conditions stability

Finally, the free-flying Helix configuration propagation is presented in Figure 12. The configuration is that reported in Figure 8 but with seven spacecrafts in total. The parameters of the configuration are reported in Table 4. It is clear that even in this case the greatest drift occurs in the Along-Track direction. The envelope of the curves goes from a maximum distance with respect to the leader of 200 m to reach about 490 m after 80 orbits (drift of 3.63 $m/orbit$).

$a \cdot \delta i$	$450\ m$
$a \cdot \delta e$	$650\ m$
α_1	$9°$

Table 4. Helix parameters for simulation.

Energy Matching (EM) Initial Conditions Method

As it has been shown in previous section the CW initial conditions are not suitable for long-duration missions. In particular, the along-track drift proved to be the main problem for the stability of the analyzed configurations, even reaching the order of hundreds meters per orbit. For the reasons above, it is clear that an alternative initialization is needed.
In order to find the solution to this problem it is necessary to find the cause of these large drifts. Firstly, it is evident that the linearization and assumptions done by CW initial conditions are the primary source of instability. The great advantage of this methodology is its simpleness in the physical interpretation thus resulting in an easy task of finding parameters which return a given configuration. In order to maintain this useful aspect, the Energy Matching (EM) Initial Conditions Method analyzes Equations 11 and finds Initial Relative Velocities for the followers which minimize the drifts by imposing no difference in energy between the spacecrafts of the formation. In order to simplify the logical process that EM method follows to find these IRVs, it is possible to approach the problem by considering the simple Keplerian dynamics. In fact, in such dynamics, it is possible to state that the period of the i-th satellite depends only on the gravitational constant and the semi-major axis of the orbit through the following relation

$$T_i = 2\pi\sqrt{\frac{a_i^3}{\mu}}$$

So, it is evident, that in Keplerian dynamics a differential semi-major axis would cause a differential period thus resulting in relative drift between the spacecrafts of the formation. The semi-major axis also defines the energy of the orbit from which the name of the method derives. In fact, if the energy (represented by a) is matched (or balanced), the

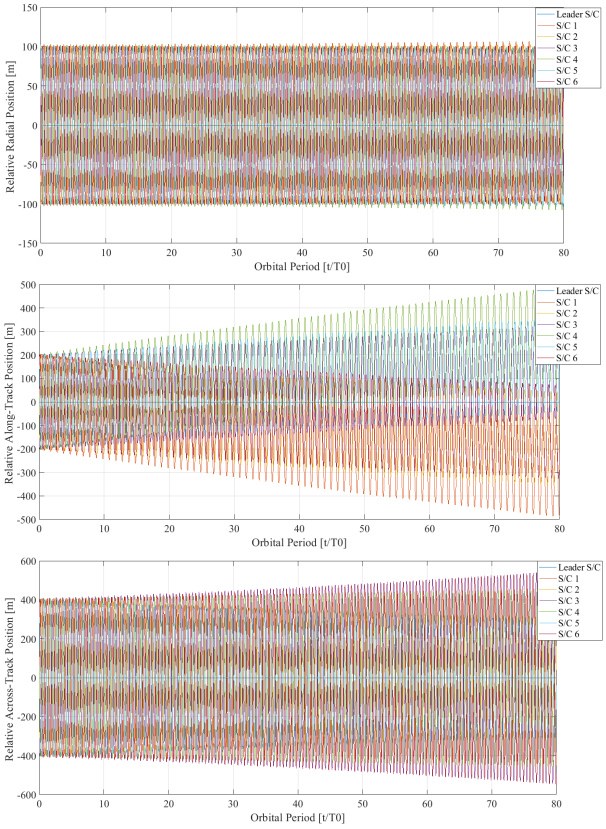

Figure 12. Helix relative dynamics propagation, CW Initial Conditions

relative drift will be reduced. Of course, the only equality of a is not sufficient to stabilize a formation which is subject to many conservative and non-conservative perturbing forces, but, if through the same procedure, the main perturbations are taken into account when calculating the energy of the spacecrafts, good results can be achieved. With these notions in mind, following sections will show how EM considering J_2 potential field will allow to find IRVs which make the formation stable for several orbits [16].

Linear Energy Matching

Analysing Equations 11 it is possible to notice that the majority of coefficients in CW equations are sinusoidal, but there are some terms which are linear in time (all the terms which are multiplied for t). These terms are those which contribute more to the drift presented in the last sections. In fact, it can be noticed how these terms are present in the second line of the matrix, i.e. in the line describing the evolution of the relative along-track direction.
For these considerations, it is possible to initialize relative velocities in order to nullify these terms, thus results in the following equation

$$\dot{y}_{LEM}(0) = -2nx(0) \tag{18}$$

where the subscript LEM stays for Linear Energy Matching. Equation 18 is sufficient to eliminate the time-linear coefficients, but, for defining completely the IRV, also $\dot{x}(0)$ and $\dot{z}(0)$ have to be initialized. If no particular initial velocities are required, a good choice which minimizes propellant is to set them to 0. So, the final conditions are

$$\begin{aligned} \dot{x}_{LEM}(0) &= 0 \\ \dot{y}_{LEM}(0) &= -2nx(0) \\ \dot{z}_{LEM}(0) &= 0 \end{aligned} \tag{19}$$

Otherwise, if a particular configuration wants to be created, $\dot{x}(0)$ and $\dot{z}(0)$ can be initialized as done in previous sections. This is a first step towards a greater stability but it is not sufficient. In fact, the equations used consider Keplerian dynamics and their efficiency drastically reduces when the satellites so initialized are subject to non-Keplerian dynamics.

Non-Linear Energy Matching

It is possible to impose Energy Matching using non-linear energy equation for Keplerian dynamics. If $\boldsymbol{V}_{NEM}$ is the absolute velocity vector of the general follower which has to be retrieved, and $\boldsymbol{V}$ is the absolute velocity of the leader spacecraft, non-linear energy matching condition holds

$$\frac{\|\boldsymbol{V}\|^2}{2} - \frac{\mu}{r} = \frac{\|\boldsymbol{V}_{NEM}\|^2}{2} - \frac{\mu}{r_{NEM}} \tag{20}$$

where r amd r_{NEM} are the norm of the inertial positions of leader and follower respectively. Equation 20 can be solved for $\|\boldsymbol{V}_{NEM}\|$, thus obtaining

$$\|\boldsymbol{V}_{NEM}\| = \sqrt{\|\boldsymbol{V}\|^2 + 2\left(\frac{\mu}{r_{NEM}} - \frac{\mu}{r}\right)} \tag{21}$$

In Keplerian dynamics, it is possible to express the vectors $\boldsymbol{V}_{NEM}$ and $\boldsymbol{V}$ in LVLH components as follows

$$\begin{aligned} \boldsymbol{V} &= v_x\hat{\boldsymbol{x}} + \frac{h}{r}\hat{\boldsymbol{y}} \\ \boldsymbol{V}_{NEM} &= \left(v_x + \dot{x}_{NEM} - y_{NEM}\omega_z\right)\hat{\boldsymbol{x}} \\ &\quad + \left(\frac{h}{r} + \dot{y}_{NEM} + x_{NEM}\omega_z\right)\hat{\boldsymbol{y}} + \dot{z}_{NEM}\hat{\boldsymbol{z}} \end{aligned}$$

where $\hat{\boldsymbol{x}}$, $\hat{\boldsymbol{y}}$, $\hat{\boldsymbol{z}}$ are the LVLH unit vectors, while v_x, h and $\omega_z = n$ are respectively the radial velocity, the angular momentum of the leader and the component in $\hat{\boldsymbol{z}}$ of the LVLH frame angular velocity. Equation 20 adds a condition on the module of the velocity vector of the follower, so if its direction is the same of Linear Energy Matching, it is possible to calculate the vector $\boldsymbol{V}_{NEM}$ through the following

$$\begin{aligned} \boldsymbol{V}_{NEM} &= \frac{\|\boldsymbol{V}_{NEM}\|}{\|\boldsymbol{V}_{LEM}\|}\boldsymbol{V}_{LEM} \\ &= \frac{\sqrt{\|\boldsymbol{V}\|^2 + 2\left(\frac{\mu}{r_{NEM}} - \frac{\mu}{r}\right)}}{\|\boldsymbol{V}_{LEM}\|}\boldsymbol{V}_{LEM} \end{aligned} \tag{22}$$

writing $\boldsymbol{V}_{LEM}$ in LVLH frame as done for $\boldsymbol{V}_{NEM}$ as follows

$$\begin{aligned} \boldsymbol{V}_{LEM} &= \left(v_x + \dot{x}_{LEM} - y_{LEM}\omega_z\right)\hat{\boldsymbol{x}} \\ &\quad + \left(\frac{h}{r} + \dot{y}_{LEM} + x_{LEM}\omega_z\right)\hat{\boldsymbol{y}} + \dot{z}_{LEM}\hat{\boldsymbol{z}} \end{aligned}$$

and substituting it in Equation 22, imposing the same initial relative position ($\boldsymbol{\rho}_{NEM} = \boldsymbol{\rho}_{LEM} = \boldsymbol{\rho}(0) = [x(0), y(0), z(0)]^T$) and evaluating for $t = 0$, the initial

relative velocity which considers non-linear energy matching is found

$$\begin{aligned}\dot{x}_{NEM}(0) &= \frac{\|\boldsymbol{V}_{NEM}\|}{\|\boldsymbol{V}_{LEM}\|}\dot{x}_{LEM}(0) \\ &+ \left(\frac{\|\boldsymbol{V}_{NEM}\|}{\|\boldsymbol{V}_{LEM}\|} - 1\right)(v_x - y(0)\omega_z) \\ \dot{y}_{NEM}(0) &= \frac{\|\boldsymbol{V}_{NEM}\|}{\|\boldsymbol{V}_{LEM}\|}\dot{y}_{LEM}(0) \\ &+ \left(\frac{\|\boldsymbol{V}_{NEM}\|}{\|\boldsymbol{V}_{LEM}\|} - 1\right)\left(\frac{h}{r_0} + x(0)\omega_z\right) \\ \dot{z}_{NEM}(0) &= \frac{\|\boldsymbol{V}_{NEM}\|}{\|\boldsymbol{V}_{LEM}\|}\dot{z}_{LEM}(0)\end{aligned} \tag{23}$$

It is possible to substitute Equations 19in Equations 23 to obtain the final version

$$\begin{aligned}\dot{x}_{NEM}(0) &= \left(\frac{\|\boldsymbol{V}_{NEM}\|}{\|\boldsymbol{V}_{LEM}\|} - 1\right)(v_x - y(0)\omega_z) \\ \dot{y}_{NEM}(0) &= \frac{\|\boldsymbol{V}_{NEM}\|}{\|\boldsymbol{V}_{LEM}\|}(-2\omega_z x(0)) \\ &+ \left(\frac{\|\boldsymbol{V}_{NEM}\|}{\|\boldsymbol{V}_{LEM}\|} - 1\right)\left(\frac{h}{r_0} + x(0)\omega_z\right) \\ \dot{z}_{NEM}(0) &= 0\end{aligned} \tag{24}$$

where r_0 represents the initial distance of the leader from the center of the Earth and $\|\boldsymbol{V}_{NEM}\|$ can be calculated through Equation 21.
The derived equations present minimal drift in all directions when the relative motion includes arbitrary eccentricity of both the leader and the followers. Instead, when the followers are initialized with Equations 24 and than propagated in a non-Keplerian dynamics the stability of the formation is still compromised. In fact, the perturbations act modifying the energy of the orbit followed by the followers thus resulting in a modification of Equation 24 and consequently all the procedure above presented is not valid anymore. [16] proposes an alternative method for initializing any leader-follower pair such that the motion is stable in an environment where the non-perfect sphericity of the earth (J_2) is considered. Since J_2 is the most important perturbation in low orbit, these initial conditions are very efficient in case of formations working in LEO and are able to maintain a good level of stability even if the dynamics with which the formation is propagated includes perturbations of minor importance (Drag, Solar Pressure, etc...).

Energy Matching including J_2 perturbation

Before explaining the procedure to impose Energy Matching including J_2, it can be useful to make some clarifications. In general, through the CW equations, the only fixed initial relative velocity is the along-track component $\dot{y}_{LEM}(0) = -2\omega_z x(0)$, the radial and across-track components, observing the Equations 11 have not to satisfy particular conditions in order to eliminate some particular drift. As they are free, they can be set to zero, as done in Equation 19 for fuel saving in deployment phase, or they can be set in order that other conditions are satisfied. In particular, [16] set them in order to reduce risk of collision (condition on $\dot{x}_{LEM}(0)$) and to reduce across-track drift due to differential RAAN (condition on $\dot{z}_{LEM}(0)$). In this case their values are

$$\dot{x}_{LEM}(0) = \frac{1}{2}\omega_z y(0) \tag{25}$$

$$\dot{z}_{LEM}(0) = -\omega_z z(0)\tan\theta_0 \tag{26}$$

where θ_0 is the initial argument of latitude of the leader spacecraft. It is possible to express Equations 25, 18 and 26 in matrix form

$$\begin{aligned}\begin{bmatrix}\dot{x}_{LEM}(0)\\ \dot{y}_{LEM}(0)\\ \dot{z}_{LEM}(0)\end{bmatrix} &= \boldsymbol{R}_{\omega_z}\begin{bmatrix}x(0)\\ y(0)\\ z(0)\end{bmatrix} \\ &= \begin{bmatrix}0 & \frac{1}{2}\omega_z & 0\\ -2\omega_z & 0 & 0\\ 0 & 0 & -\omega_z\tan\theta_0\end{bmatrix}\begin{bmatrix}x(0)\\ y(0)\\ z(0)\end{bmatrix}\end{aligned} \tag{27}$$

For simplicity of equations, in this work, Equation 27 will be used as the starting point for the development of the Non-Linear EM with J_2 method, but, in general, the steps that will be presented can be performed perfectly in the same way in the case where it is possible to express the initial relative velocities as linear functions in the relative initial positions, i.e. in the following way

$$\begin{bmatrix}\dot{x}_{LEM}(0)\\ \dot{y}_{LEM}(0)\\ \dot{z}_{LEM}(0)\end{bmatrix} = \begin{bmatrix}a_1 & a_2 & a_3\\ -2\omega_z & 0 & 0\\ b_1 & b_2 & b_3\end{bmatrix}\begin{bmatrix}x(0)\\ y(0)\\ z(0)\end{bmatrix} \tag{28}$$

where $a_1, a_2, a_3, b_1, b_2, b_3$ are arbitrary constants chosen following different criteria. After detailing this aspect, it is possible to derive EM in case of presence of J_2 perturbation. After the central body perturbation the main effect on an orbiting satellite of the gravity potential is that due to first zonal coefficient J_2. Thanks to conservative property of the force field generated by gravity potential, it is possible to write the gravity potential and its gradient truncated to consider up to J_2 term as follows [15]

$$U_{J2} = -\frac{\mu}{r} - \frac{k_{J_2}}{r^3}\left(\frac{1}{3} - \sin^2 i\sin^2\theta\right) \tag{29}$$

$$\begin{aligned}\nabla U_{J2} &= \frac{\mu}{r^2}\hat{\boldsymbol{x}} + \frac{k_{J_2}}{r^4}\left(1 - 3\sin^2 i\sin^2\theta\right)\hat{\boldsymbol{x}} \\ &+ \frac{k_{J_2}\sin^2 i\sin 2\theta}{r^4}\hat{\boldsymbol{y}} + \frac{k_{J_2}\sin 2i\sin\theta}{r^4}\hat{\boldsymbol{z}}\end{aligned}$$

where $k_{J_2} = \frac{3}{2}J_2\mu R_e^2$ and R_e is the reference Earth radius, i and θ are the inclination and argument of latitude of the considered spacecraft. U_{J_2} represents the energy of a satellite subject to J_2 potential field. It can be noticed that ∇U_{J_2} is not aligned with the radial given by the unit vector $\hat{\boldsymbol{x}}$ of the LVLH. This aspect is important because, Equation 27 is written in a frame which is aligned with the force acting on the LVLH frame, and in order to exploit it properly, a frame aligned with ∇U_{J_2} has to be considered. If we consider a frame in which its unit vector $\hat{\boldsymbol{x}}'$ is aligned with ∇U_{J_2} and $\hat{\boldsymbol{y}}'$ remains in the orbital plane, it is possible to transform a generic vector described in the LVLH frame into this new frame by two rotations, a counterclockwise rotation about the $\hat{\boldsymbol{z}}$ axis by the angle α, resulting in the intermediate frame of unit vectors $\hat{\tilde{\boldsymbol{x}}}, \hat{\tilde{\boldsymbol{y}}}, \hat{\tilde{\boldsymbol{z}}}$, and a second rotation β about the $\hat{\tilde{\boldsymbol{y}}}$ axis. In equations, the rotation matrix which allows to describe a general vector in LVLH into $[\hat{\boldsymbol{x}}', \hat{\boldsymbol{y}}', \hat{\boldsymbol{x}}']$ (U_{J_2} frame) can be written as

$$\boldsymbol{R}_{U_{J_2},L} = \begin{bmatrix}c_\alpha c_\beta & s_\alpha c_\beta & s_\beta\\ -s_\alpha & c_\alpha & 0\\ -c_\alpha s_\beta & -s_\alpha s_\beta & c_\beta\end{bmatrix} \tag{30}$$

where $s_x = \sin(x)$ and $c_x = \cos(x)$, and α and β are given by the following

$$\alpha = \arctan\left(\frac{\nabla U_{J2}\cdot\hat{\boldsymbol{y}}}{\nabla U_{J2}\cdot\hat{\boldsymbol{x}}}\right)$$

$$\beta = \arctan\left(\frac{\nabla U_{J2}\cdot\hat{\boldsymbol{z}}}{\sqrt{\left(\nabla U_{J2}\cdot\hat{\boldsymbol{x}}\right)^2+\left(\nabla U_{J2}\cdot\hat{\boldsymbol{y}}\right)^2}}\right)$$

It is now possible to impose relation 27 in the U_{J_2} frame and then to retrieve the components in LVLH frame through 30, thus obtaining

$$\begin{aligned}\begin{bmatrix}\dot{x}'_{LEMJ_2}(0)\\ \dot{y}'_{LEMJ_2}(0)\\ \dot{z}'_{LEMJ_2}(0)\end{bmatrix} &= \begin{bmatrix}0 & \frac{1}{2}\omega_z & 0\\ -2\omega_z & 0 & 0\\ 0 & 0 & -\omega_z\tan\theta_0\end{bmatrix}\begin{bmatrix}x'(0)\\ y'(0)\\ z'(0)\end{bmatrix}\\ &= \boldsymbol{R}_{\omega_z}\boldsymbol{R}_{U_{J_2},L}\begin{bmatrix}x(0)\\ y(0)\\ z(0)\end{bmatrix}\end{aligned} \tag{31}$$

and $\boldsymbol{R}_{\omega_z}\boldsymbol{R}_{U_{J_2},L}$ equals

$$\begin{bmatrix}-\frac{1}{2}\omega_z s_\alpha & \frac{1}{2}\omega_z c_\alpha & 0\\ -2\omega_z c_\alpha c_\beta & -2\omega_z s_\alpha c_\beta & -2\omega_z s_\beta\\ \omega_z c_\alpha s_\beta\tan\theta_0 & \omega_z s_\alpha s_\beta\tan\theta_0 & -\omega_z c_\beta\tan\theta_0\end{bmatrix}$$

where in this case $\omega_z \neq n$ but $\omega_z = \sqrt{\frac{\|\nabla U_{J_2}\|}{r}}$ because the LVLH is also subject to J_2 perturbation [15]. Initial vector of velocity $[\dot{x}'_{LEMJ_2}(0), \dot{y}'_{LEMJ_2}(0), \dot{z}'_{LEMJ_2}(0)]^T$ can be also rotated in LVLH frame in order to obtain IRV in LVLH frame

$$\begin{aligned}\begin{bmatrix}\dot{x}_{LEMJ_2}(0)\\ \dot{y}_{LEMJ_2}(0)\\ \dot{z}_{LEMJ_2}(0)\end{bmatrix} &= \boldsymbol{R}_{L,U_{J_2}}\begin{bmatrix}\dot{x}'_{LEMJ_2}(0)\\ \dot{y}'_{LEMJ_2}(0)\\ \dot{z}'_{LEMJ_2}(0)\end{bmatrix}\\ &= \boldsymbol{R}^T_{U_{J_2},L}\begin{bmatrix}\dot{x}'_{LEMJ_2}(0)\\ \dot{y}'_{LEMJ_2}(0)\\ \dot{z}'_{LEMJ_2}(0)\end{bmatrix}\\ &= \boldsymbol{R}^T_{U_{J_2},L}\boldsymbol{R}_{\omega_z}\boldsymbol{R}_{U_{J_2},L}\begin{bmatrix}x(0)\\ y(0)\\ z(0)\end{bmatrix}\end{aligned} \tag{32}$$

Equation 32 simply considers the linearized conditions but in the U_{J_2} frame the Energy Matching condition still needs to be imposed. If we now consider the energy of a generic follower as described by relative quantities instead of absolute ones as done in Equation 29 which will be used for the leader spacecraft (or LVLH frame) the following holds

$$U_{EMJ_2} = -\frac{\mu}{r_{EMJ_2}} - \frac{k_{J_2}}{r^3_{EMJ_2}}\left(\frac{1}{3} - \frac{(r+x)\sin i\sin\theta + y\sin i\cos\theta + z\cos i}{r^2_{EMJ_2}}\right)$$

it is possible to write the Energy Matching considering J_2 perturbation as

$$\|\boldsymbol{V}_{EMJ_2}\| = \sqrt{\|\boldsymbol{V}\|^2 + 2\left(U_{EMJ_2} - U\right)}$$

where U is the energy of the leader spacecraft and expressed by Equation 29. It is possible to follow the same passages done in the previous section but considering that the velocity of the follower as described in a LVLH frame subject to J_2 ([15]) can be written as

$$\begin{aligned}\boldsymbol{V}_{EMJ_2} =& \left(v_x + \dot{x}_{EMJ_2} - y_{EMJ_2}\omega_z\right)\hat{\boldsymbol{x}}\\ &+ \left(\frac{h}{r} + \dot{y}_{EMJ_2} + x_{EMJ_2}\omega_z - z_{EMJ_2}\omega_x\right)\hat{\boldsymbol{y}}\\ &+ \left(\dot{z}_{EMJ_2} + y_{EMJ_2}\omega_x\right)\hat{\boldsymbol{z}}\end{aligned}$$

in this case $\omega_x \neq 0$ because of the J_2 perturbation [15]. The components $\dot{x}_{EMJ_2}$,$\dot{y}_{EMJ_2}$,$\dot{z}_{EMJ_2}$ can be found by imposing that Equation 32 satisfy

$$\begin{aligned}\boldsymbol{V}_{EMJ_2} &= \frac{\|\boldsymbol{V}_{EMJ_2}\|}{\|\boldsymbol{V}_{LEMJ_2}\|}\boldsymbol{V}_{LEMJ_2}\\ &= \frac{\sqrt{\|\boldsymbol{V}\|^2 + 2\left(U_{EMJ_2} - U\right)}}{\|\boldsymbol{V}_{LEMJ_2}\|}\boldsymbol{V}_{LEMJ_2}\end{aligned} \tag{33}$$

Developing both sides of Equation 33, using Equation 32 and evaluating it at $t = 0$, the initial relative velocity conditions described in the LVLH frame subject to J_2 perturbation can be found

$$\begin{aligned}\dot{x}_{EMJ_2}(0) =& -\frac{\|\boldsymbol{V}_{EMJ_2}\|}{\|\boldsymbol{V}_{LEMJ_2}\|}\Bigg[\left(\frac{3}{2}c_\alpha s_\alpha c_\beta - c^2_\alpha s^2_\beta t_{\theta_0}\right)x(0)\\ &+ \left(\frac{1}{2}c^2_\alpha c_\beta + 2s^2_\alpha c_\beta - c_\alpha s_\alpha s^2_\beta t_{\theta_0}\right)y(0)\\ &+ \left(2s_\alpha s_\beta + c_\alpha c_\beta s_\beta t_{\theta_0}\right)z(0)\Bigg]\omega_z\\ &+ \left(\frac{\|\boldsymbol{V}_{EMJ_2}\|}{\|\boldsymbol{V}_{LEMJ_2}\|} - 1\right)\left(v_x - y(0)\omega_z\right)\end{aligned}$$

$$\begin{aligned}\dot{y}_{EMJ_2}(0) =& \frac{\|\boldsymbol{V}_{EMJ_2}\|}{\|\boldsymbol{V}_{LEMJ_2}\|}\\ &\Bigg[\left(-2c^2_\alpha c_\beta - \frac{1}{2}s^2_\alpha c_\beta - c_\alpha s_\alpha s^2_\beta t_{\theta_0}\right)x(0)\\ &+ \left(-\frac{3}{2}c_\alpha s_\alpha c_\beta - s^2_\alpha s^2_\beta t_{\theta_0}\right)y(0)\\ &+ \left(-2c_\alpha s_\beta + s_\alpha c_\beta s_\beta t_{\theta_0}\right)z(0)\Bigg]\omega_z\\ &+ \left(\frac{\|\boldsymbol{V}_{EMJ_2}\|}{\|\boldsymbol{V}_{LEMJ_2}\|} - 1\right)\left(\frac{h}{r} + x(0)\omega_z - z(0)\omega_x\right)\end{aligned}$$

$$\begin{aligned}\dot{z}_{EMJ_2}(0) =& \frac{\|\boldsymbol{V}_{EMJ_2}\|}{\|\boldsymbol{V}_{LEMJ_2}\|}\Bigg[\left(-\frac{1}{2}s_\alpha s_\beta + c_\alpha c_\beta s_\beta t_{\theta_0}\right)x(0)\\ &+ \left(\frac{1}{2}c_\alpha s_\beta + s_\alpha c_\beta s_\beta t_{\theta_0}\right)y(0)\\ &+ \left(-c^2_\beta t_{\theta_0}\right)z(0)\Bigg]\omega_z\\ &+ \left(\frac{\|\boldsymbol{V}_{EMJ_2}\|}{\|\boldsymbol{V}_{LEMJ_2}\|} - 1\right)y(0)\omega_x\end{aligned} \tag{34}$$

Equation 34 defines the Initial Relative Velocity of a generic follower in LVLH components which minimize relative drifts in all directions when J_2 perturbation is considered. In the

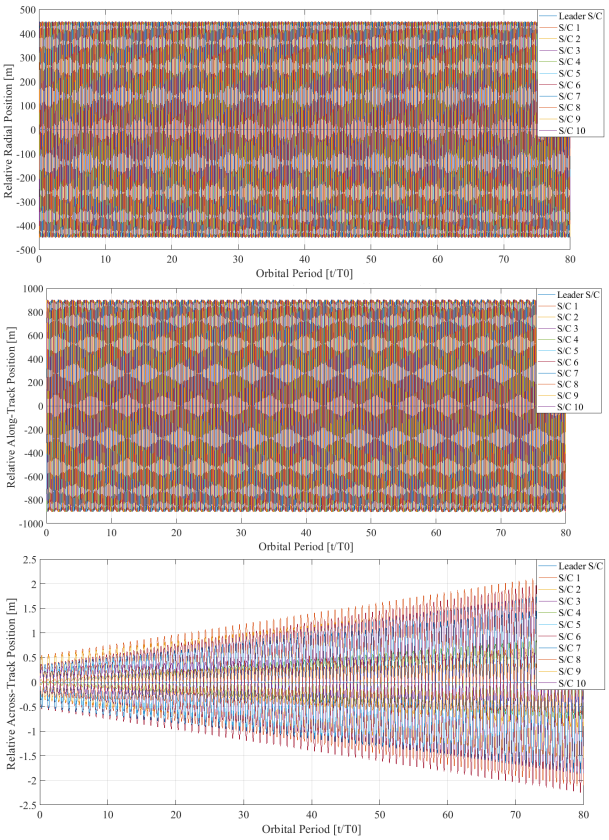

Figure 13. IC relative dynamics propagation, EM J_2 Initial Conditions

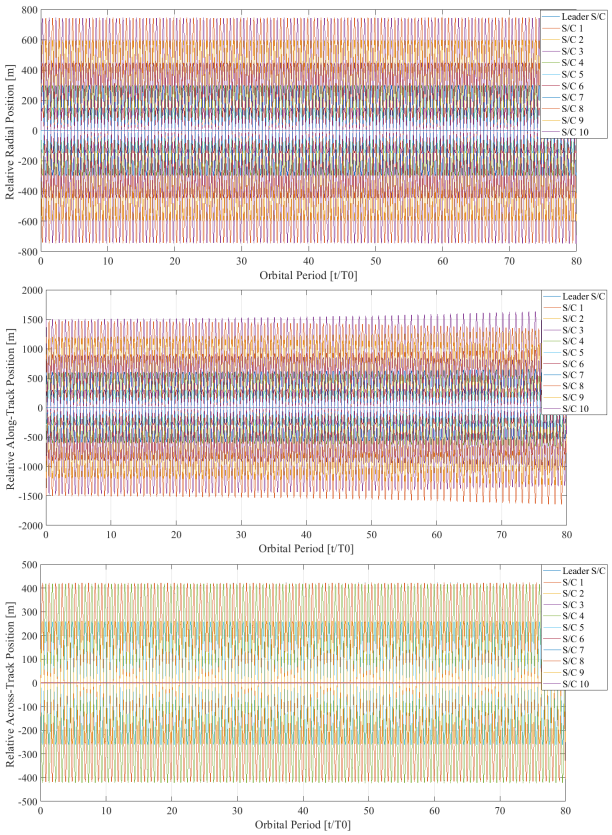

Figure 14. CT relative dynamics propagation, EM J_2 Initial Conditions

next section, the stability of the presented configurations initialized with Equation 34 will be analyzed and compared with results obtained in Section. 3.

Stability of the EM including J_2 Initial Conditions

The aim of this section is to show the efficacy of Equations 34 with respect to the initialization of the formation through CW Equations To do so properly, exactly the same parameters of the simulations showed in Section. 3 have been used, in particular the leader initial orbital elements are those presented in Table 1, and Initial Relative Positions of the followers in the different configurations are the same reported in Figures 2, 3, 4. Figures 13, 14 and 15 report the results of the simulations for all the analyzed configurations. It is evident that EM Initial Conditions improve the stability of the formations, the envelopes remain nearly the same after 80 orbits. The only case in which relative drift is more evident, regards across-track direction of IC configuration, but it remains very limited showing a relative drift of about $0.03\ m/orbit$.

It has to be underlined that, even if the stability has been improved, Equations 34 tend to give higher Initial Relative Velocities, thus resulting in larger oscillations in relative positions and consequently higher risk of collision. For this reason, when controlling the formation (section 4), Collision Avoidance strategies have to be used for the safety of the mission.
After hundreds orbits, minor perturbations start to destabilize the formation (i.e. differential Drag), and Formation Control becomes necessary to maintain high system performances.

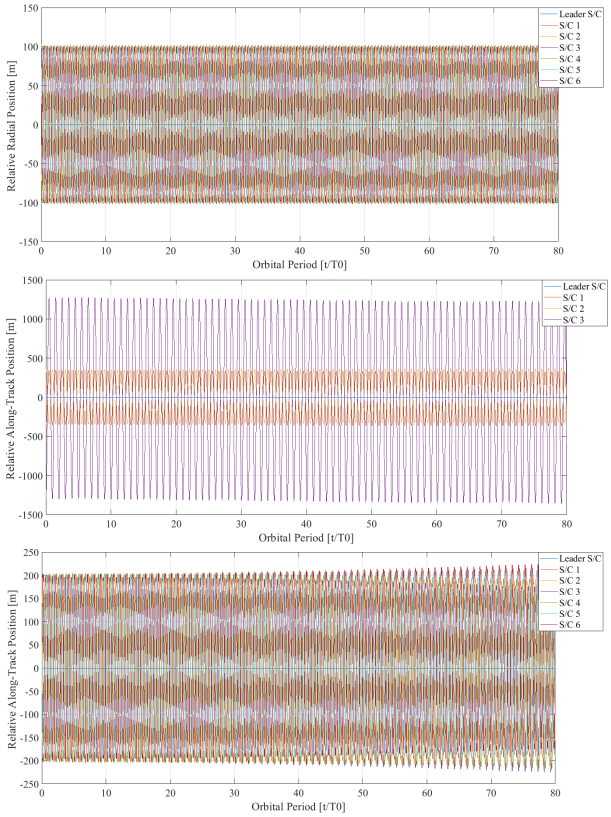

Figure 15. Helix relative dynamics propagation, EM J_2 Initial Conditions

4. FORMATION CONTROL

Definition of the General Optimal Control Problem

The goal is to solve an optimization problem in order to find optimal control forces and torques which are able to minimize energy actuation consumption for the 6DoF dynamics. For reasons which will be better explained later, two different optimization problems, one for translational dynamics and one for rotational are derived. In addition, to avoid being too repetitive, the discussion will be carried out considering a de-centralized architecture, in which all satellites are equipped with sufficient computational resources to be able to independently calculate their optimal trajectory. Calling $\boldsymbol{x}(t) = [\boldsymbol{\rho}^T(t), \dot{\boldsymbol{\rho}}^T(t)]^T$ the translational state vector and $\boldsymbol{u}(t) = [u_x(t), u_y(t), u_z(t)]^T$ the control input, the general non-linear optimization problem can be written for the i-th spacecraft as in Problem 1.

Problem 1 *Translational case, Non-linear Optimal Control*

$$\min_{\boldsymbol{u}_i(t)} \int_0^{t_f} \|\boldsymbol{u}_i(t)\|_2 \, dt$$

subject to

$$\begin{aligned}
\dot{\boldsymbol{x}}_i(t) &= f\left(\boldsymbol{x}_i(t), \boldsymbol{u}_i(t)\right) && \forall t \in [0, t_f] \\
\|\boldsymbol{u}_i(t)\|_2 &\leq U_{\max} && \forall t \in [0, t_f] \\
\|C\left[\boldsymbol{x}_i(t) - \boldsymbol{x}_j(t)\right]\|_2 &\geq R_{\text{col}} && \begin{matrix} \forall t \in [0, t_f] \\ j = 1, \ldots, N \\ j \neq i \end{matrix} \\
\boldsymbol{x}_i(0) &= \boldsymbol{x}_{i,0} \\
\boldsymbol{x}_i\left(t_f\right) &= \boldsymbol{x}_{i,f}
\end{aligned}$$

---

where t_f represents the final time at which the reconfiguration ends, f represents the controlled dynamics where the dependence on the state of LVLH frame (or chief) has been omitted, U_{max} is the maximum available thrust (considering that spacecrafts are equipped with single thrust [8]), N is the total number of spacecrafts, R_{col} is the minimum distance required for collision avoidance, $\boldsymbol{x}_{i,0}$ and $\boldsymbol{x}_{i,f}$ are respectively the initial and final state vector conditions, while $C = [\boldsymbol{I}_{3\times3}, \boldsymbol{0}_{3\times3}]$ just extracts the relative positions from the state vector.
Analogously, it is possible to express the optimization problem in case of rotational motion. If $\boldsymbol{x}(t) = [\boldsymbol{q}^T(t), \dot{\boldsymbol{\omega}}^T(t)]^T$ is the state vector and $\boldsymbol{g}(t) = [g_x(t), g_y(t), g_z(t)]^T$ is the control input, for i-th spacecraft, it is possible to derive Problem 2.

Problem 2 *Rotational case, Non-linear Optimal Control*

$$\min_{\boldsymbol{g}_i(t)} \int_0^{t_f} \|\boldsymbol{g}_i(t)\|_2 \, dt$$

subject to

$$\begin{aligned}
\dot{\boldsymbol{x}}_i(t) &= f\left(\boldsymbol{\rho}_i, \dot{\boldsymbol{\rho}}_i, \boldsymbol{x}_i(t), \boldsymbol{g}_i(t)\right) && \forall t \in [0, t_f] \\
\|\boldsymbol{g}_i(t)\|_2 &\leq \tau_{\max} && \forall t \in [0, t_f] \\
\boldsymbol{x}_i(0) &= \boldsymbol{x}_{i,0} \\
\boldsymbol{x}_i\left(t_f\right) &= \boldsymbol{x}_{i,f}
\end{aligned}$$

---

where τ_{max} is the saturation of the actuator and the dependence of the rotational dynamics on relative positions and velocities has been highlighted (external torques depend on accelerations and accelerations depend on absolute position and velocity of the vector).
Problems 1 and 2 try to minimize the integral over an interval of time of the norm of the control inputs. This is in line with the fact that fuel consumption is related to this quantity, so the objective functions considered represent indirectly the cost of fuel consumption. The presented problems are non-linear and constrained optimization problem. They are difficult to solve, also by indirect methods which can take a very long run time. A solution often adopted is that one to make to re-enter the problem in the so-called convex optimization problems for which convex programming succeeds to guarantee times of resolution much lower.

Convexification of the Optimal Control Problem

Convex programming imposes that the treated problem is expressed as

$$\begin{aligned}
\text{minimize} \quad & J\left(\boldsymbol{Z}\right) \\
\text{subject to} \quad & g_j\left(\boldsymbol{Z}\right) \leq 0, \quad j = 1, \cdots, l \\
& \boldsymbol{a}_i{}^T \boldsymbol{Z} - \boldsymbol{b}_i = 0, \quad i = 1, \cdots, m
\end{aligned} \tag{35}$$

where the vector $\boldsymbol{Z}$ is the variable to optimize, g_j are convex functions while the equality constraints $\boldsymbol{a}_i{}^T \boldsymbol{Z} - \boldsymbol{b}_i = 0$ are expressed as affine functions. In order to reduce Problems 1 and 2 to the problem given by (35), it is necessary to linearize the dynamics and discretize the continuous problem in order to identify a single vector to optimize.

Linearization of the Dynamics

It is possible to approximate the non-linear dynamics of the system by using a reference trajectory through Taylor expansion. If only the first term of this expansion is considered the resulting approximation function is linear. Considering the Problem 1, if we call $\overline{\boldsymbol{x}}_i(t)$ the reference trajectory and $\overline{\boldsymbol{u}}_i(t)$ the reference control law (for Problem 2 the considerations are exactly the same), the linearized dynamics can be written as

$$\dot{\boldsymbol{x}}_i(t) = A_i(t)\boldsymbol{x}_i(t) + B_i(t)\boldsymbol{u}_i(t) + c_i\left(t\right) \tag{36}$$

where $A_i(t) = \left.\frac{\partial f}{\partial \boldsymbol{x}_i}\right|_{\overline{\boldsymbol{x}}_i(t), \overline{\boldsymbol{u}}_i(t)}$, $B_i(t) = \left.\frac{\partial f}{\partial \boldsymbol{u}_i}\right|_{\overline{\boldsymbol{x}}_i(t), \hat{\boldsymbol{u}}_i(t)}$ and $c(t) = f(\overline{\boldsymbol{x}}_i(t), \overline{\boldsymbol{u}}_i(t)) - A_i(t)\overline{\boldsymbol{x}}_i(t) - B_i(t)\overline{\boldsymbol{u}}_i(t)$. The main problem is that Equation 36 requires reference trajectories and the more distant this reference will be from the real value of the trajectory the coarser the approximation will be resulting in a lower accuracy in reaching the final state. This problem will be solved by adopting the sequential convex programming explained in the next sections.

Discretization

The optimization time interval $[0, t_f]$ is discretized in K points. t_k is the time in the k-th point and, $\Delta t_k = t_{k+1} - t_k$ is the k-th interval of time. In this work, an equispaced discretization has been used so $\Delta t_k = \Delta t \quad \forall k = 0, 1, \cdots, K-1$ thus resulting also in $t_f = K\Delta t$. We can now apply this discretization to Problem 1 starting from the cost-function. The integral becomes a sum over the time-interval

$$\sum_{k=0}^{K-1} \|\boldsymbol{u}_i^k\|_2 \tag{37}$$

where $\boldsymbol{u}_i^k = \boldsymbol{u}_i(t_k)$, while the dynamics can be written as follows

$$\dot{\boldsymbol{x}}_i^{k+1} = A_i^k \boldsymbol{x}_i^k + B_i^k \boldsymbol{u}_i^k + c_i^k \qquad k = 0, 1, \cdots, K-1 \quad (38)$$

where $\boldsymbol{x}_i^k = \boldsymbol{x}_i(t_k)$ and

$$\begin{aligned} A_i^k &= e^{A_i(t_k)\Delta t} \\ B_i^k &= \int_0^{\Delta t} e^{A_i(t_k)\tilde{t}} B(\tilde{t}) d\tilde{t} \\ c_i^k &= \int_0^{\Delta t} e^{A_i(t_k)\tilde{t}} c(\tilde{t}) d\tilde{t} \end{aligned} \quad (39)$$

Following the same reasoning, it is possible to write directly the Problem 2 in a convexified form

---

Problem 3 *Rotational case, Convex Optimal Control*

$$\min_{\boldsymbol{g}_i} \sum_{k=0}^{K-1} \|\boldsymbol{g}_i^k\|_2$$

subject to

$$\dot{\boldsymbol{x}}_i^{k+1} = A_i^k \boldsymbol{x}_i^k + B_i^k \boldsymbol{g}_i^k + c_i^k \qquad k = 0, 1, \cdots, K-1$$

$$\left\|\boldsymbol{g}_i^k\right\|_2 \leq \tau_{\max} \qquad k = 0, 1, \cdots, K-1$$

$$\boldsymbol{x}_i^0 = \boldsymbol{x}_{i,0}$$

$$\boldsymbol{x}_i^K = \boldsymbol{x}_{i,f}$$

Remark:
Concerning rotational case, the derivation of matrices A_i^k and B_i^k is slight different from previous case. In fact, as highlighted before, i-th spacecraft rotational dynamics depends also on $\boldsymbol{\rho}_i$ and $\dot{\boldsymbol{\rho}}_i$, thus resulting in the need of translational reference trajectories ($\overline{\boldsymbol{\rho}}_i(t)$ and $\overline{\dot{\boldsymbol{\rho}}}_i(t)$) for the computation of the first-order Taylor expansion, so that $A_i(t) = \frac{\partial f}{\partial \boldsymbol{x}_i}\Big|_{\overline{\boldsymbol{x}}_i(t), \overline{\boldsymbol{u}}_i(t), \overline{\boldsymbol{\rho}}_i(t), \overline{\dot{\boldsymbol{\rho}}}_i(t)}$, $B_i(t) = \frac{\partial f}{\partial \boldsymbol{u}_i}\Big|_{\overline{\boldsymbol{x}}_i(t), \overline{\boldsymbol{u}}_i(t), \overline{\boldsymbol{\rho}}_i(t), \overline{\dot{\boldsymbol{\rho}}}_i(t)}$ and $c(t) = f(\overline{\boldsymbol{x}}_i(t), \overline{\boldsymbol{u}}_i(t), \overline{\boldsymbol{\rho}}_i(t), \overline{\dot{\boldsymbol{\rho}}}_i(t)) - A_i(t)\overline{\boldsymbol{x}}_i(t) - B_i(t)\overline{\boldsymbol{u}}_i(t)$ The discretization process does not change with respect to the translational case.

It is now more evident the reasons why the choice of writing two different problems, one for translational motion and one for rotational, has been taken. In general, a single problem involving all variables for 6DoF dynamics could be derived, thus resulting in a very huge problem increasing the difficulty of finding the solution. By splitting this single problem into two sub-problems allows to control only one typology motion without solving the other. For example, if the formation pointing has to be corrected without controlling translational motion, it is possible to solve problems 2 or 3 by linearizing the dynamics about the free-flying translational motion (from Equations 10). This results in a lower computational effort. Problem 3 is a convex problem. In fact if we define the optimization variable for the i-th spacecraft as $\boldsymbol{Z}_i$ as $\boldsymbol{Z}_i = [(\boldsymbol{x}_i^0)^T, \cdots (\boldsymbol{x}_i^K)^T, (\boldsymbol{g}_i^0)^T, \cdots, (\boldsymbol{g}_i^{K-1})^T]^T$, all the constraints and cost-function can be re-written with the formalism of Equation 35. Concerning Problem 2, the Collision Avoidance constraint makes the problem still non-convex. In addition, it requires the knowledge of the position of all the spacecrafts for all instants $\boldsymbol{x}_i^k$ which is a complicated aspect. If a centralized strategy is adopted, the task is simpler because the chief can calculate all the trajectories and then send them to each spacecraft considering the CA constraint. Instead, if a de-centralized strategy is adopted, each spacecraft should calculate its optimal trajectory without CA constraint, send this to the chief and then receive all other trajectories in order to add CA constraint and re-calculate the optimal trajectory.

Convexification of Collision Avoidance Constraint

The convexification of CA constraint follows the procedure adopted by [8]. It is possible to show that a sufficient condition for the non-convex CA constraint is the following

$$\left(\overline{\boldsymbol{x}}_i^k - \overline{\boldsymbol{x}}_j^k\right)^T C^T C \left(\boldsymbol{x}_i^k - \boldsymbol{x}_j^k\right) \geq R_{\text{col}} \left\|C\left(\overline{\boldsymbol{x}}_i^k - \overline{\boldsymbol{x}}_j^k\right)\right\|_2 \quad (40)$$

where $\overline{\boldsymbol{x}}_i$ is an initial guess trajectory for the i-th spacecraft.

Remark:
Previous equation implies that the spacecraft performing the optimization should know trajectories of all the satellites. This is not verified in case of de-centralized strategy where each satellite optimizes its own trajectory. For this reason the constraint just presented needs to be changed so that we can have a CA requirement in this strategy as well. This problem can be solved by changing Equation 40 in

$$\left(\overline{\boldsymbol{x}}_i^k - \overline{\boldsymbol{x}}_j^k\right)^T C^T C \left(\boldsymbol{x}_i^k - \overline{\boldsymbol{x}}_j^k\right) \geq R_{\text{col}} \left\|C\left(\overline{\boldsymbol{x}}_i^k - \overline{\boldsymbol{x}}_j^k\right)\right\|_2$$

which implies that also the trajectory of the j-th spacecraft is estimated. This problem is not present in centralized strategy where the optimization involves all the spacecrafts. This procedure allows to make Problem 2 solvable through convex programming. However, two negative aspects are still present. The first is that this methodology makes the solution of the problem a potentially sub-optimal solution, in fact, by increasing the volume of forbidden space, solutions that could present a lower cost-function are discarded. The second is that guess trajectories are necessary. These trajectories can be obtained in different ways. The choice that has been made in this work, consists, in the case of de-centralized architecture, in solving the optimization problem at least two times. The first solution does not consider the CA constraint and the second uses the trajectories found in the first one as guess trajectories in order to include the CA convex constraint. In the case of centralized architecture, the procedure is the same, but in this case there is no need for the frequent passage of information between satellites, only after all optimal trajectories have been calculated, the satellites receive the control inputs.

Sequential Convex Programming (SCP)

Several approximations were introduced during the convexification of Problem 1. First, the introduction of initial guess trajectories $\overline{\boldsymbol{x}}_i$ for linearization can lead to significant errors. Moreover, if the initial trajectories deviate a lot from the real ones, the constraint on the CA may result in the elimination of solutions that could in reality satisfy the minimum distance criterion and consequently the solution thus obtained would deviate even further from the optimal one. In order to solve this problem, the Sequential Convex Programming (SCP) method is used. As the name suggests, SCP involves a sequential and iterative resolution of the problem, trying to refine the solution more and more until a certain accuracy is satisfied. The idea behind SCP is simple, if $\boldsymbol{x}_{i,m-1}$ represents the solution of the problem at (m-1)-th iteration, it is possible to use this solution as the new reference trajectory for iteration (m)-th $\overline{\boldsymbol{x}}_i = \boldsymbol{x}_{i,m-1}$. At this point, one criterion is needed to stop the iterative process. The most

used and the most intuitive would be to stop the process in the case in which the new iteration does not differ more than a predetermined quantity from the previous one, this can be written through the following equation

$$\|\boldsymbol{x}_{i,m}^k - \boldsymbol{x}_{i,m-1}^k\|_\infty < \epsilon \qquad \forall k = 0, \cdots, K$$

where ϵ is a constant and it is chosen depending on the desired accuracy.

After calculating these trajectories, Problem 3 can be solved for controlling rotational motion with higher precision. The problem of this method is that it does not consider unmodeled disturbances or errors in the application of control. In fact, having no external measurements this method still represents an open-loop control. This can lead to non-negligible errors in the reached final state. In order to close the loop, the method of Closed Loop control with Sequential Convex Programming (CL-SCP) will be described in the following section.

Closed Loop Control with Sequential Convex Programming (CL-SCP)

The concept behind (CL-SCP) algorithm is very simple and is based on classical characteristics of a feedback control loop. If relative measurements are available, it is possible to re-initialize the optimization problem by using the measurements as the new initial state vectors. This is equal to closing the control loop as in a feedback controller. If the re-initialization is applied several times during the maneuvers the final result will more accurate. If we call k_0 the instant at which the re-initialization is applied and K_H the optimization horizon of the single CL-SCP iteration, it is possible to rewrite Problem 1 in the final convex form by considering re-initialization as

---

Problem 4 *Translational case, De-centralized Convex Optimal Control for CL-SCP*

$$\min_{\boldsymbol{u}_i} \sum_{k=k_0}^{K-1} \|\boldsymbol{u}_i^k\|_2$$

subject to

$$\dot{\boldsymbol{x}}_i^{k+1} = A_i^k \boldsymbol{x}_i^k + B_i^k \boldsymbol{u}_i^k + c_i^k \qquad k = k_0, \cdots, K-1$$

$$\left\|\boldsymbol{u}_i^k\right\|_2 \leq U_{\max} \qquad k = k_0, \cdots, K-1$$

$$\begin{array}{c} \left(\overline{\boldsymbol{x}}_i^k - \overline{\boldsymbol{x}}_j^k\right)^T C^T C \left(\boldsymbol{x}_i^k - \overline{\boldsymbol{x}}_j^k\right) \\ \geq R_{\text{col}} \left\|C\left(\overline{\boldsymbol{x}}_i^k - \overline{\boldsymbol{x}}_j^k\right)\right\|_2 \end{array} \quad \begin{array}{c} k = k_0, \cdots, k_0 + K_H \\ j = 1, \ldots, N \\ j \neq i \end{array}$$

$$\boldsymbol{x}_i^0 = \boldsymbol{x}_{i,actual}$$

$$\boldsymbol{x}_i^K = \boldsymbol{x}_{i,f}$$

---

where $\boldsymbol{x}_{i,actual}$ is the measured state at k_0. It is clear how Problem 4 is simpler to solve. In particular, the most time-spending part of optimal control is due to CA constraints, in Problem 6 the constraints is considered only up to $k_0 + K_H$, while it is evident that the control input has to be calculated in all the time span K which is the instant at which the final position $\boldsymbol{x}_{i,f}$ has to be reached.
It can be remarked that the smaller is the horizon K_H the more the trajectory followed will be optimal but the greater will be the computational effort. The choice of K_H depends also on the total time used for the correction t_f and will always be dictated by a trade-off between precision and available computational resources. Before passing to the numerical results, it is necessary to make some clarifications. Problem 4 is written in the context of a de-centralized strategy. This implies that the i-th spacecraft optimizes its own trajectory regardless of the position and/or velocity of others. This strategy, which is more suitable in the case where the satellites of the formation are all equipped with the same computational resources, does not consider the optimization of the formation as a single entity which is what we would be most interested in. In fact, if instead of the cost-function $\min_{\boldsymbol{u}_i} \sum_{k=0}^{K-1} \|\boldsymbol{u}_i^k\|_2$ we had $\min_{[\boldsymbol{u}_1, \cdots, \boldsymbol{u}_N]} \sum_{i=1}^{N} \sum_{k=0}^{K-1} \|\boldsymbol{u}_i^k\|_2$, where N is the number of spacecrafts, the optimization would choose a path that would minimize the overall fuel consumption. This, as demonstrated in [8], results in a more efficient use of the fuel consumption, so it can be affirmed that, if a satellite can be endowed with a high-performances data handling system, this solution is to prefer with respect to to de-centralized one.

5. NUMERICAL RESULTS

This section aims at presenting some test cases simulations based on the methods and algorithms presented in section 4. Concerning Optimal control, simulations of different strategies (centralized, de-centralize, SCP only and CL-SCP) will be presented to show different performances in terms of accuracy, computational time and fuel efficiency. In the first section, common parameters used for all simulations are presented, while specific parameters are described for each simulation in the relative section.

Common Parameters

Common parameters involve the initial conditions of the leader spacecraft which are reported in Table 1

The simulations have been carried out on different configurations, parameters relative to each one of these configurations will be detailed in the next sections. In all cases, the formation is composed by spacecrafts with the same initial inertial properties and dimensions (cubic satellites have been considered) which are detailed in Table 5.
All simulations have been carried out considering unmodeled perturbations. These effects are taken into account by considering the applied control inputs as gaussian random variables with properties detailed in Table 6 which also reports actuators saturation values.
As far as the propulsion system is concerned, in the simulations a cold gas system with an $I_{sp} = 70\ s$ has been considered to control the translational dynamics, while as far as the rotational one is concerned, the control is done by reaction wheels whose dynamics is neglected and whose only parameter considered is the maximum torque they can generate (as in Table 6). Finally, the simulations consider all perturbations presented previously.

Drift Correction

In this simulation, a Helix configuration composed by seven spacecrafts (leader included) has been propagated in free-flying configuration until a condition activates the control

Initial mass	m_0	$20\ kg$
Inertia matrix	$\boldsymbol{J}_{G,BF}$	$diag([0.3, 0.3, 0.3])\ kg \cdot m^2$
Length	a	$0.3\ m$

Table 5. Initial inertial properties and dimensions

Force actuator saturation	$F_{i,max}\ i = x, y, z$	$1\ N$
Control force average	μ_F	$0\ N$
Control force standard deviation	σ_F	$2 \times 10^{-2}\ N$
Torque actuator saturation	$\tau_{i,max}\ i = x, y, z$	$1\ N \cdot m$
Control torque average	μ_τ	$0\ N \cdot m$
Control torque standard deviation	σ_τ	$10^{-4}\ N \cdot m$

Table 6. Actuators properties

loop. It is possible to adopt different criteria to activate control algorithms, the one chosen in this work activates the control loop when the euclidean distance of a generic follower with respect to the leader is higher than a predetermined value. This value depends on the configuration and on the maximum admissible drift the formation can undergo while remaining operational.
The drift correction simulation has been chosen to show differences between methods presented in Section 4, in particular, the same configuration has been controlled in 6DoF with the optimal controller centralized architecture in SCP and in de-centralized architecture both in SCP and CL-SCP. The initial conditions of the spacecrafts of the formation are dictated by the propagation in uncontrolled mode until the control algorithm is activated by the criterion explained above, while the final relative positions are the same as reported in Table 7 and initial relative velocities have been found with Equation 34 for improving stability. Concerning rotational motion, also in this case the initial state depends on the history of perturbations acting during the propagation while the final state is the same for all the spacecrafts and considers an Earth pointing direction for attitude and $\boldsymbol{\omega}_{BF} = \mathbf{0}$.

Optimal Controller de-centralized SCP

The parameters used for all Optimal control simulations are reported in Table 8.

In Figure 16 optimal trajectories as calculated by Optimal controller in de-centralized strategy using sequential convex programming are calculated. It is visible how, using the dynamics in order to save fuel, the trajectories are homogeneous and smooth. These trajectories are obtained through

$a \cdot \delta i$	$100\ m$
$a \cdot \delta e$	$200\ m$
α_1	$9°$
N	7

Table 7. Helix final parameters for drift corrction simulation.

Final time	t_f	$0.05T_0\ s$
Number of points	K	100
Stopping criterion	ϵ	10^{-2}
Minimum distance	R_{col}	$20\ m$
Initial guess trajectories	$\overline{\boldsymbol{x}}_i^k$	free-flying leader trajectory $\forall i, k$
Initial guess control inputs	$\overline{\boldsymbol{u}}_i^k$	$0\ \forall i, k$

Table 8. SCP simulation paramters

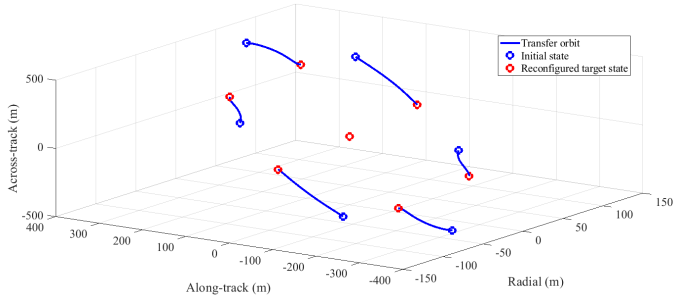

Figure 16. Trajectories drift correction Optimal controller de-centralized SCP

control forces presented in Figure 17. The control forces are symmetrical with respect to the time axis and optimal controller predicts smaller radial control forces F_x than in the other two directions.

In this case the total fuel consumption is $\Delta m_{tot} = 0.410259\ kg$, while the average is $\Delta m_{av} = 0.0683765\ kg$. A more in-depth comparative analysis will be done in a later section.

Optimal Controller centralized SCP

The centralized case simulation has been effectuated in order to analyze the effects of adopting a different architecture. The calculated trajectories are not reported because they are very similar to the de-centralized case, they both present the smoothness of Optimal control trajectories.

Regarding convergence behavior there are not relevant remarks. The actuation forces are not reported because they are similar to the de-centralized case. What is more interesting is the total fuel consumption which is of $\Delta m_{tot} = 0.404724\ kg$. Showing that centralized strategy is able to further optimize trajectories with respect to de-centralized case as anticipated previously, this effect is not very visible when the number of satellites is low while it is much more evident when the formation is composed of hundreds or more satellites. Regarding computational times, Table 9 indicates the CPU time taken to find the final trajectories. It should be noted that in the de-centralized case, the value shown in the table is the average computation time taken by a single satellite. In fact, the total time of the simulation, which is carried out for the entire formation, has been divided by the number of satellites that make up the formation. It is evident how de-centralized strategy allows to calculate trajectories in a shorter interval of time, underlying that the choice of the architecture is dictated by a trade-off between fuel consumption and computational resources. In this case the average fuel consumption is

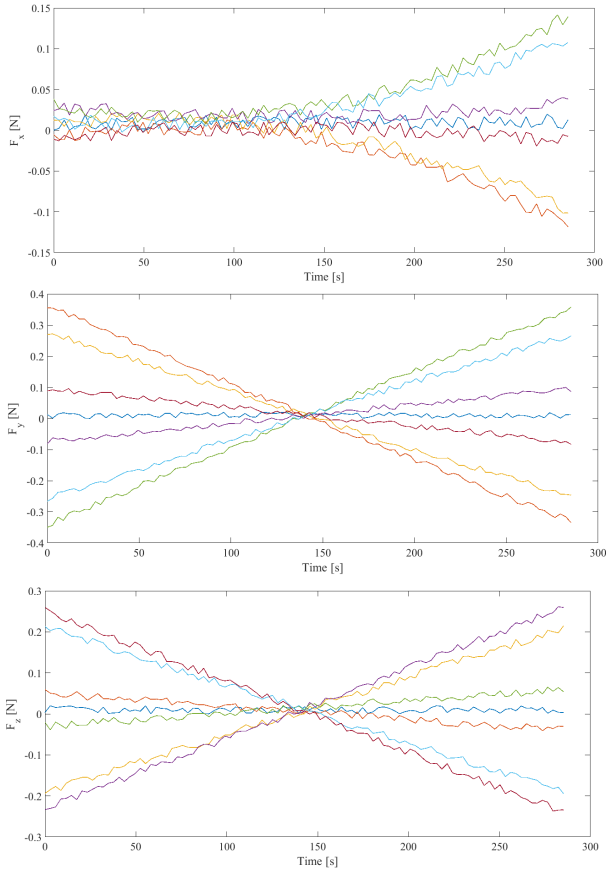

Figure 17. Actuation Forces drift correction Optimal controller de-centralized SCP

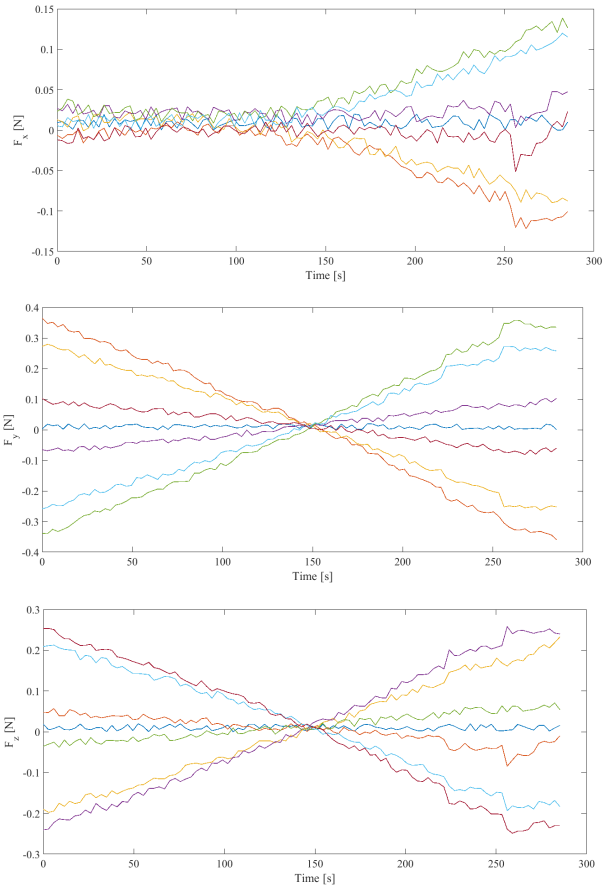

Figure 18. Actuation Forces drift correction Optimal controller de-centralized CL-SCP

Centralized strategy	$115.7343\ s$
De-entralized strategy	$26,3616\ s$

Table 9. Computational times comparison

$\Delta m_{av} = 0.067454\ kg$.

Optimal Controller de-centralized CL-SCP

Parameters used for this simulation are the same of the Table 8 and only the definition of the CL-SCP horizon $K_H = 12$ was added. The propagation of the trajectories is not reported because the differences from the decentralized case would not be appreciable. In Figure 18, control input forces are reported for completeness, not showing any particular appreciable difference from previous optimal control cases. The most interesting thing is that in this case the final position error has been reduced a lot with respect to the Open Loop case. This is the main reason why an Open Loop control system cannot meet the accuracy requirements of the mission. Figure 19 show qualitatively a detailed comparison in xy plane between de-centralized OL and CL strategies. It is clear how the final position obtained through the closed loop strategy is nearer to the required one for all the spacecrafts. These results will be also quantitatively analyzed in the next section. Concerning rotational motion, Figures 20, 21 and 22 report the evolution of the quaternions and angular velocities and the control torques obtained through the Optimal control algorithm.
From Figures 20 and 21 attitude and angular velocity errors are presented. In Figure 22 it is immediately visible

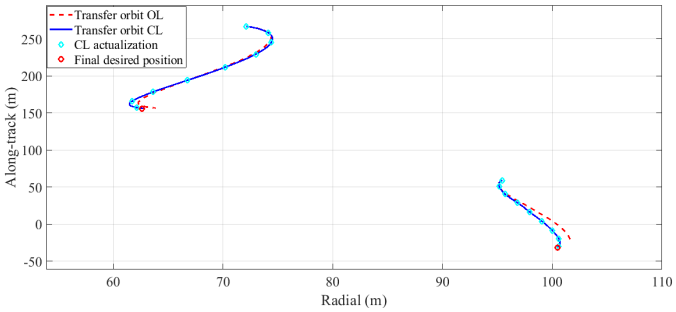

Figure 19. xy trajectories comparison between SCP and CL-SCP (detail)

how also in this case the trend of control torques are more homogeneous and above all are of the order of $10^{-3}\ Nm$, proving the effective optimization of the rotational trajectories. Regarding fuel consumption this simulation presents $\Delta m_{tot} = 0.439086\ kg$ and the average is $\Delta m_{av} = 0.073181\ kg$.

Conclusions drift correction

It is now possible to make a discussion about the results that have just been found in the case of correcting drifts of the initial configuration. In particular, it is possible to compare the different methodologies applied considering the accuracy with which the final target state was reached and the fuel consumption of the manoeuvre. In terms of accuracy, this

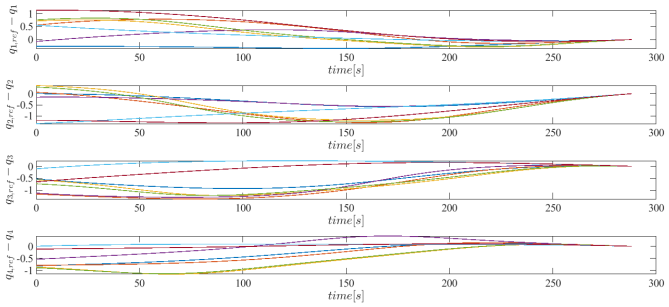

Figure 20. Quaternion errors history drift correction Optimal controller CL-SCP

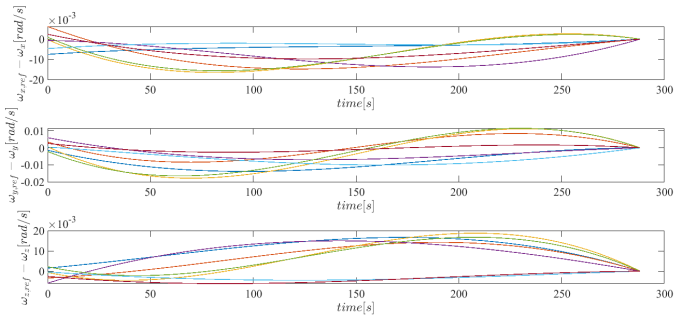

Figure 21. Angular velocity errors history drift correction Optimal controller CL-SCP

work has rather focused on the analysis of reaching the final reached position of the spacecrafts (same considerations can be done with velocities, quaternions and angular velocities). The metric chosen for this comparison is the euclidean distance between the final position of the spacecraft and the desired final position

$$\Delta\rho = \sqrt{(\rho_{x,ref} - \rho_x)^2 + (\rho_{y,ref} - \rho_y)^2 + (\rho_{z,ref} - \rho_z)^2}$$

In Table 10 the results of this quantity for each simulations have been reported in terms of maximum position error and the average one calculated considering all the formation. It is evident that the optimal control cases in de-centralized and non-centralized SCP are the worst cases. This result was predictable considering that they are Open-Loop methodologies that do not consider external measures, so linearization errors and unmodeled perturbations have more important effects. Finally, it is important to underline how the closing of the loop in the case of Optimal control has gained an order of magnitude in reaching the final position. The final error is due to the fact that at a certain point the remaining part of the instants in which the optimal calculation is performed is smaller than the horizon K_H, so the last part of the trajectories is propagated without further updating the initial states through the measurements. The precision with which the final state is reached is very important because the stability of the configuration depends on it. If the final conditions have been imposed in such a way that the satellites are placed in J_2 invariant orbits, an error in position or velocity with respect to these conditions will cause a higher drift rate and consequently a greater need for corrections. In Table 11, the fuel consumption of each simulation has been reported in terms of total mass used by the whole formation Δm_{tot}, the average one Δm_{av} and the percentage of the average mass

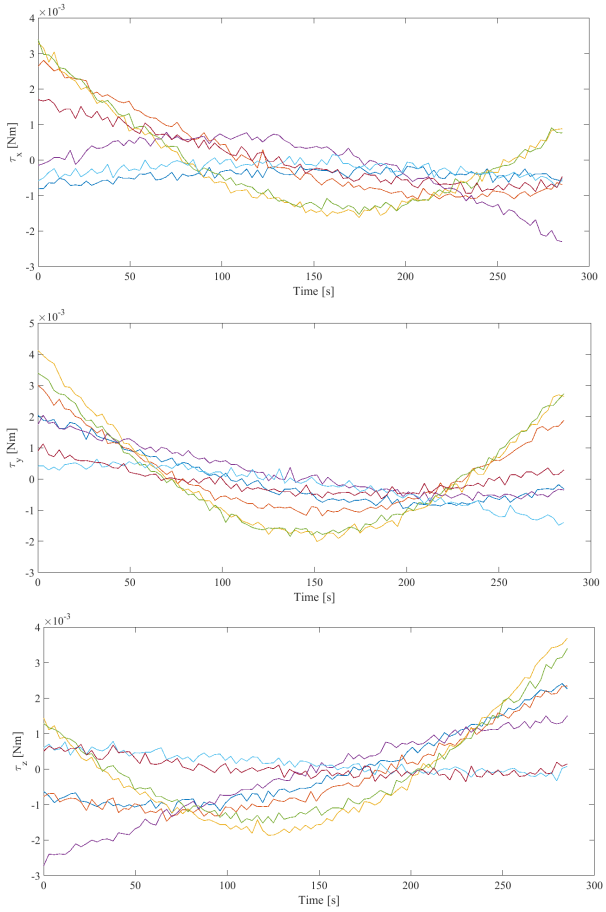

Figure 22. Actuation Torques drift correction Optimal controller CL-SCP

OC dec SCP	$\Delta\rho\ [m]$
Maximum	8.6289
Average	4.52795

OC cen SCP	$\Delta\rho\ [m]$
Maximum	4.7097
Average	3.3175

OC dec CL-SCP	$\Delta\rho\ [m]$
Maximum	0.7887
Average	0.6207

Table 10. Final position errors drift corrections simulations

with respect to the initial one $\Delta m_{\%av} = \Delta m_{av}/m_0 \cdot 100$. The de-centralized strategy obtains very good results but finds however a sub-optimal solution since each satellite does not know a priori the position of the other spacecrafts, which instead the centralized strategy does. In fact, if only one spacecraft could calculate all the trajectories, it would be able to plan the control forces in order to avoid collisions in a preventive way. The centralized strategy reduces the fuel used, but it has still the problem of accuracy. A good compromise is the de-centralized strategy in Closed-Loop. In fact, it increases the accuracy of the system but at the expense of greater fuel use than the simple de-centralized strategy. This is due to the fact that the actual trajectory followed by the spacecrafts is not the one calculated by Optimal control, and consequently, a trajectory that requires more corrections (sub-optimal trajectory).

Case	$\Delta m_{tot}\ [kg]$	$\Delta m_{av}\ [kg]$	$\Delta m_{\%av}$
OC dec SCP	0.410259	0.0683765	0.3418825
OC cen SCP	0.404724	0.067454	0.33727
OC dec CL-SCP	0.439086	0.073181	0.365905

Table 11. Fuel consumption summary drift corrections simulations

6. CONCLUSIONS

This research tries to give a complete overview on formation flying. The main aspects of this kind of systems have been presented starting from the requirements the propagation model should have in order to properly deal with relative dynamics to the control of the formation by using an optimal controller in different strategies. Problems related to the management of such a system, like fuel consumption and computational cost, gave a definite direction to the discussion that had as main objective to present the state of the art of methods that try to mitigate such problems. In particular, the study of formation stability, which led to the synthesis of initial conditions that guarantee the smallest possible drift, is essential for a long duration missions and for a higher quality of data taken. Despite the importance of the study of stability, it has been seen that it is not sufficient to eliminate the drift of the followers with respect to the leader, so it is necessary to provide strategies for active control of the formation. In this work, the attention has been brought to the Optimal controller whose purpose is to calculate the control inputs in order to minimize a given objective function. Normal methods of solving a non-linear optimization problem would take too long to find the solution if computational capabilities are limited. It is for this reason that, in order to be able to implement optimal computation in autonomous systems, the problem has been convexified and finally solved in very limited time through Sequential Convex Programming. Optimal controller does not normally take into account possible external measures with which the boundary conditions of the problem to be solved can be updated. In order to increase its effectiveness, optimal control was periodically solved using external measures obtained from a propagation of the full non-linear dynamics with the control actions computed in the previous iteration. Optimal controller gave satisfying results in terms of accuracy even in cases where unmodeled perturbations and in general external disturbances act on the system. It is also important to underline that the type of architecture chosen for the mission, is closely linked to the choice of algorithm for the calculation of formation control that must also be based on the type of sensors and communication system which the formation spacecrafts are equipped with.

ACKNOWLEDGMENTS

©2021 California Institute of Technology. Government sponsorship acknowledged. This research was carried out at the Jet Propulsion Laboratory, California Institute of Technology, under a contract with the National Aeronautics and Space Administration.

REFERENCES

[1] Mazouz, R., Quadrelli, M., Beauchamp, R. (2021, March). Dynamics and Optimal Control for Free-Flight and Tethered Arrays in Low Earth Orbit. In 2021 IEEE Aerospace Conference (50100) (pp. 1-20). IEEE.

[2] Montenbruck, O., Gill, E., Lutze, F. (2002). Satellite orbits: models, methods, and applications. Appl. Mech. Rev., 55(2), B27-B28.

[3] Szmuk M., Acikmese B., Andrew W. Berning Jr., Huntington G. (2016). Successive Convexification for Fuel-Optimal Powered Landing with Aerodynamic Drag and Non-Convex Constraints. AIAA Guidance, Navigation, and Control Conference, San Diego, CA.

[4] Curtis H.D. (2010). Orbital Mechanics for Engineering Students. Elsevier - Butterworth-Heinemann.

[5] Quadrelli M. (2000). Modeling and dynamics of tethered formations for space interferometry. 11th AAS/AIAA Space Flight Mechanics Meeting, Santa Barbara, California, Oct. 2000.

[6] Fasano G., D'Errico M. (2009). Modeling orbital relative motion to enable formation design from application requirements. Celest Mech Dyn Astr, pp. 113-139.

[7] Gim D. W., Alfriend K.T. (2003). State Transition Matrix of Relative Motion for the Perturbed Noncircular Reference Orbit. Journal of Guidance, Control, and Dynamics Vol. 26, No. 6.

[8] Sarno S., Guo G., D'Errico M., Gill E. (2020). A guidance approach to satellite formation reconfiguration based on convex optimization and genetic algorithms. Adv. Space Res.

[9] Carrer L., Bovolo F., Bruzzone L. (2019). Distributed Radar Sounder: A Novel Concept for Subsurface Investigations Using Sensors in Formation Flight. IEEE Transactions on Geoscience and Remote Sensing, Vol. 57, No. 12.

[10] Sullivan J., Grimberg S., D'Amico S. (2017). Comprehensive Survey and Assessment of Spacecraft Relative Motion Dynamics Models, .Journal of Guidance, Control, and Dynamics, pp. 1837-1859.

[11] Segal S., Gurfil P. (2009). Effect of Kinematic Rotation-Translation Coupling on Relative Spacecraft Translational Dynamics. Journal of Guidance, Control, and Dynamics, vol. 32, no. 3, pp. 1045–1050.

[12] Quadrelli M.B., Ono M., Jain A.(2016). Modeling of Active Tether System concepts for planetary exploration. Acta Astronautica.

[13] Quadrelli M. (2001). Modeling and Dynamics of Tethered Formations for Space Interferometry. Paper AAS 01-231.

[14] Quadrelli M. (2003). Effect of Distributed Rod and String Flexibility on Formation Dynamic Stability. Journal of the Astronautical Sciences, Vol. 51, No.3, pp.339-357.

[15] Xu G., Wang D. (2008). Nonlinear Dynamic Equations of Satellite Relative Motion Around an Oblate Earth. Journal of Guidance, Control, and Dynamics, Vol. 31, No. 5, pp. 1521-1524.

[16] Morgan D., Chung S., Blackmore L., Acikmese B., Bayard D., Hadaeghk F.Y. (2021). Swarm-Keeping Strategies for Spacecraft under J2 and Atmospheric Drag Perturbations. American Institute of Aeronautics and Astronautics.

[17] Krieger G., Moreira A., Fiedler H., Hajnsek I., Werner M., Younis M., Zink M. (2007). TanDEM-X: A Satellite Formation for High-Resolution SAR Interferometry. IEEE Transactions on Geoscience and Remote Sensing.

[18] Kechichian J.A. (1998). Motion in General Elliptic Or-

bit with Respect to a Dragging and Precessing Coordinate Frame. The Journal of the Astronautical Sciences, pp. 25-45.

[19] Segal S., Carmi A., Gurfil P. (2013). Stereovision-Based Estimation of Relative Dynamics Between Noncooperative Satellites: Theory and Experiments. IEEE Transactions on Control Systems Technology.

[20] Xing Y., Cao X., Zhang S., Guo H., Wang F. (2010). Relative position and attitude estimation for satellite formation with coupled translational and rotational dynamics. Acta Astronautica.

[21] Alfriend K., Vadali S.R., Gurfil P., How J., Breger L. (2010). Spacecraft Formation Flying. Dynamics, Control and Navigation. Elsevier.

[22] Lopez-Dekker P., Krieger G., Moreira A. (2012). Multistatic Radar Systems. Springer.

[23] Clohessy W.H., Wiltshire R.S. (1960). Terminal guidance system for satellite rendezvous. Journal of the Aerospace Sciences. 27, 9,pp. 653-658.

[24] Grant M., Boyd S. (2014). CVX: Matlab software for disciplined convex programming, version 2.1.

[25] Hughes, S. P., Qureshi, R. H., Cooley, S. D., Parker, J. J. (2014). Verification and validation of the general mission analysis tool (GMAT). AIAA/AAS astrodynamics specialist conference, 4151.

[26] Morgan D. and Chung S., Hadaegh F.Y. (2014). Model predictive control of swarms of spacecraft using sequential convex programming. Journal of Guidance, Control, and Dynamics. 37, 6, pp. 1725-1740. American Institute of Aeronautics and Astronautics.

[27] Singgih Pulukadang M. howpublished = "https://www.slideshare.net/AmitRastogi11/synthetic-aperture-radar".

[28] Rasotto, M., Morselli, A., Wittig, A., Massari, M., Di Lizia, P., Armellin, R., Ortega, G. (2016). Differential algebra space toolbox for nonlinear uncertainty propagation in space dynamics.

[29] Yue X., Wang X., Dai H. (2014). A simple time domain collocation method to precisely search for the periodic orbits of satellite relative motion. Mathematical Problems in Engineering. Hindawi.

[30] Programmazione Lineare Intera. howpublished = "http://www.diag.uniroma1.it/ or/meccanica/cap12.pdf".

BIOGRAPHY

Riccardo Apa *received his bachelor's degree in aerospace engineering from Politecnico di Torino. After performing the first year of the master in the same institute, he won the "Double Degree" competition which led him to obtain, in addition to the master degree from Politecnico di Torino, the title "Diplôme d'ingenieur" at ISAE-Supaero. His research interests include control of distributed dynamic systems, trajectory optimization, space debris monitoring and machine learning applications in the space sector.*

Marco B. Quadrelli *is an internationally renowned expert in modeling for dynamics and control of complex space systems. He has a Master Degree in Aeronautics and Astronautics from MIT and a PhD in Aerospace Engineering from Georgia Tech. He was a visiting scientist at the Harvard- Smithsonian Center for Astrophysics, and a lecturer at the Caltech Graduate Aeronautical Laboratories. After joining NASA JPL in 1997 he has contributed to a number of flight projects including the Cassini-Huygens Probe, Deep Space One, the Mars Aerobot Test Program, the Mars Exploration Rovers, the Space Interferometry Mission, the Autonomous Rendezvous Experiment, and the Mars Science Laboratory, among others. He has been the Attitude Control lead of the Jupiter Icy Moons Orbiter Project, and the Integrated Modeling Task Manager for the Laser Interferometer Space Antenna. He has led or participated in several independent research and development projects in the areas of computational micromechanics, dynamics and control of tethered space systems, formation flying, inflatable apertures, hypersonic entry, precision landing, flexible multibody dynamics, guidance, navigation and control of spacecraft swarms, terramechanics, and precision pointing for optical systems. He is an Associate Fellow of the American Institute of Aeronautics and Astronautics, a NASA Institute of Advanced Concepts Fellow, and a Caltech/Keck Institute for Space Studies Fellow.*

Robert M. Beauchamp *received the B.S. from the University of Massachusetts Amherst, Amherst, MA, the M.S. from Northeastern University, Boston, MA, and the Ph.D. from Colorado State University, Fort Collins, CO, all in electrical engineering. Dr. Beauchamp is a radar systems engineer at the Jet Propulsion Laboratory, California Institute of Technology. His research interests include radar systems and advanced signal processing techniques with a focus on atmospheric and subsurface sounding applications.*